HIV-1 Envelope glycoprotein modulates CXCR4 clustering and dynamics on the T cell membrane

Adriana Quijada-Freire[1], César A. Santiago[2], Eva Mª García-Cuesta[1], Blanca Soler-Palacios[1], Rosa Ayala-Bueno[1], Sofía R. Gardeta[1], Enara San Sebastian[3], Eva Armendariz-Burgoa[4], María C. Puertas[4], Ricardo Villares[1], Urtzi Garaigorta[3], Luis Ignacio González-Granado[5,6], José Miguel Rodríguez-Frade[1], Jakub Chojnacki[4,7,8], Javier Martinez-Picado[4,7,9,10], Mario Mellado[1*]

[1]Chemokine Signaling group, Department of Immunology and Oncology, Centro Nacional de Biotecnología/CSIC, Campus de Cantoblanco, 28049, Madrid, Spain

[2]X-ray Crystallography Unit, Department of Macromolecules Structure, Centro Nacional de Biotecnología/CSIC, Campus de Cantoblanco, 28049, Madrid, Spain

[3]Departamento de Biología Molecular y Celular, Centro Nacional de Biotecnología/CSIC Campus de Cantoblanco, 28049, Madrid, Spain.

[4]IrsiCaixa, 08916, Badalona, Spain.

[5]12 de Octubre Health Research Institute (imas12), E-28012 Madrid, Spain.

[6]Department of Public Health School of Medicine, School of Medicine Universidad Complutense de Madrid, E-28040 Madrid, Spain.

[7]CIBERINFEC, 28029, Madrid, Spain

[8]Germans Trias i Pujol Research Institute (IGTP), 08916, Badalona, Spain

[9]University of Vic-Central University of Catalonia, 08500, Vic, Spain

[10]Catalan Institution for Research and Advanced Studies (ICREA), 08010 Barcelona, Spain.

[*]Corresponding author: Mario Mellado, Department of Immunology and Oncology, CNB/CSIC, Darwin 3, Cantoblanco, 28049 Madrid Spain. Tel: (+34) 91/585-4852; Fax: (+34) 91/372-0493; e-mail: mmellado@cnb.csic.es

Abstract

HIV-1 entry into susceptible cells requires the dynamic interaction of its envelope (Env) glycoprotein with the host cell receptor CD4 and a co-receptor, either CCR5 or CXCR4. While the molecular mechanisms of Env-receptor interactions that lead to membrane fusion have been extensively studied, the precise nanoscale redistribution of these co-receptors to viral binding sites remains unknown. In this study, we employed single-particle tracking total internal reflection fluorescence (SPT-TIRF) microscopy to quantitatively analyze nanoscale organizational changes of CXCR4 on $CD4^+$ T cell surfaces following binding of X4-tropic HIV-1. Our data reveal that both recombinant X4-gp120 and virus-like particles (VLPs) expressing physiological levels of X4 Env proteins (gp120 and gp41) promote CXCR4 clustering, a phenomenon linked to cell infection. Furthermore, these ligands induced oligomerization of $CXCR4^{R334X}$, a naturally occurring mutant of CXCR4 associated with WHIM syndrome that fails to oligomerize upon CXCL12 binding but nonetheless supports HIV-1 infection. Our findings establish a connection between CXCR4 clustering and HIV-1 infection, enhancing our understanding of the initial events in viral attachment and entry. These results further suggest that HIV-1 infection necessitates a specific spatial arrangement of co-receptors, distinct from that induced by their natural chemokine ligands, highlighting the critical role of cell-surface receptor spatial organization in cellular function.

Introduction

HIV-1 infects immune cells through a dynamic interaction between its envelope glycoprotein complex (Env), composed of gp41 and gp120 trimers [1,2], and two receptors on target cells: the primary receptor CD4, and a co-receptor, either CCR5 or CXCR4. These co-receptors are critical for viral entry infection and determine viral tropism. R5 strains (M-tropic) infect primary macrophages and certain memory $CD4^+$ T cells by binding to CD4 and CCR5[3], while X4 strains (T-tropic) infect primary $CD4^+$ T cells by binding to CD4 and CXCR4 [4].

R5-tropic viruses are typically the primary mode of transmission in humans and remain prevalent throughout the infection [5]. However, in many infected individuals, the virus evolves its tropism over time, progressing from R5-tropic to dual-tropic (R5/X4), and ultimately to X4-tropic as the infection advances [6]. This shift in tropism is associated with a more rapid decline in $CD4^+$ T cell counts [7]. Furthermore, CXCR4 has been implicated in the infection of hematopoietic progenitor cells, potentially contributing to the establishment of long-lasting latent HIV-1 reservoirs [8].

The fusion of viral and cellular membranes is initiated by the binding of gp120 to CD4 [9,10], which triggers a conformational change in gp120, enabling it to bind to co-receptors [11]. These structural changes expose the N-terminal hydrophobic fusion peptide of gp41, which then inserts into the cell membrane [12] facilitating the creation of a fusion pore and the delivery of viral material into the target cell.

Numerous studies, including those employing structural analysis, have examined the HIV-1 infection process. These studies have clarified the structural requirements and changes in gp120 and gp41 that enable membrane fusion and viral entry [13–16]. Early investigations into host cell components revealed that HIV-1 infection induces the redistribution of cell-surface CD4 and co-receptors to the sites of viral attachment [17,18].

More recent evidence, obtained through super-resolution microscopy, demonstrates that HIV-1 binding triggers CD4 clustering, a phenomenon also observed (albeit to a lesser degree) following gp120 stimulation [19]. However, less is known about which specific co-receptors are also recruited to the virus particles bound to the cell surface. It has been reported that gp120 mediates the association of CD4 with both CXCR4 and CCR5 [17,20,21]. Furthermore, it has been shown that the co-expression of CCR5 modifies the conformation of both CXCR4 homodimers and CD4/CXCR4 heterodimers. This conformational change prevents the binding of gp120 from an X4 HIV-1 strain, specifically $gp120_{IIIB}$, to the resulting CD4/CXCR4/CCR5 complex [22].

Large-scale molecular assemblies at the cell membrane, also known as signaling clusters, are increasingly recognized as key regulators of cell signaling [23]. Evidence indicates that the spatial reorganization and distribution of membrane receptors are key to controlling cell functions. Notably, clustering also appears to be essential for viral infection. For instance, Env–CD4 complexes form clusters and ring-like structures, facilitating closer contact between opposing membranes [24]. These clusters often represent a significant portion of the overall signaling process and are frequently associated with the cytoskeleton [23]. For example, CD4 receptors exist in pre-clustered structures that enlarge upon T cell activation, thereby modulating the strength of the signaling response [25,26]. Moreover, CXCR4 is organized at the cell membrane as monomers, dimers and small aggregates (groups of ≥3 receptors) called nanoclusters. The binding of its specific ligand, CXCL12, leads to a decrease in the proportion of monomers/dimers, while simultaneously increasing the formation of larger nanoclusters. This change in receptor organization consequently alters the lateral mobility of CXCR4 within the cell membrane [27]. This mechanism is critical for initiating CXCR4 signaling and enabling cells to accurately orient themselves in response to CXCL12 gradients [28]. A naturally occurring

99 CXCR4 mutant, $CXCR4^{R334X}$, which is responsible for WHIM syndrome, a severe
100 immunological disorder [29], cannot form these large nanoclusters upon CXCL12
101 binding. As a result, cells carrying this mutation lose their ability to properly sense
102 chemoattractant gradients [28].

103 Here, we employed quantitative single-particle tracking in total internal
104 reflection fluorescence (SPT-TIRF) microscopy to investigate the spatial arrangement
105 and dynamic activity of CXCR4 when exposed to HIV-1 glycoproteins. Our findings
106 reveal that both recombinant X4-gp120 and virus-like particles (VLPs) containing a
107 limited number of X4 Env proteins (gp120 and gp41) promote CXCR4 clustering on
108 cells expressing CD4 and CXCR4. Moreover, they also trigger the oligomerization of
109 $CXCR4^{R334X}$. These results suggest that, along with CD4 clustering, the
110 conformational changes in chemokine receptors triggered by HIV-1 are essential for
111 cell infection and differ from the effects of the natural ligand, CXCL12. Therefore,
112 CD4/CXCR4 complexes and their interaction sites represent potentially valuable
113 targets for developing novel therapeutic strategies to block HIV-1 entry.

114
115

116

117 **Materials and methods**

118 ***Cells and reagents***

119 HEK-293T cells, Jurkat human leukemia cells (JKCD4$^-$X4$^+$), and Daudi cells were
120 obtained from the American Type Culture Collection (CRL-3216, CRL-10915 and
121 CCL- 213, respectively; ATCC, Rockville, MD). HEK-293CD4, Jurkat CD4$^+$ cells
122 (JKCD4$^+$X4$^+$), and Jurkat cells expressing an X4-tropic HIV-1 Env (JKHXBC2) were
123 kindly provided by Drs. G. del Real (Instituto Nacional de Investigación y Tecnología
124 Agraria y Alimentaria, Madrid, Spain) and J. Alcamí (Centro Nacional de Microbiología,
125 Instituto de Salud Carlos III, Madrid, Spain). Where indicated, Jurkat cells lacking
126 endogenous *CXCR4* (JKCD4$^+$X4$^-$) [30] were electroporated with plasmids expressing wild-
127 type CXCR4-AcGFP or mutant CXCR4^{R334X}-AcGFP receptors (20 μg), as described [30].
128 Stable Jurkat cells expressing CXCR4^{R334X} (JKCD4$^+$CXCR4^{R334X}) were generated by
129 electroporation with CXCR4^{R334X} and antibiotic selection [30].

130 Human peripheral blood mononuclear cells (PBMCs) were isolated from the
131 blood of a WHIM patient (CXCR4^{R334X}) or of healthy donors, and when required from
132 buffy coats of healthy donors, which were obtained from the Centro de Transfusiones
133 (Comunidad Autónoma de Madrid, Spain) by centrifugation through Percoll density
134 gradients (760 × g, 45 min, room temperature [RT]). CD4$^+$ cells were purified by negative
135 selection using Dynabeads (Invitrogen, Thermo Fisher Scientific, Waltham, MA) and
136 activated *in vitro* for 1 week with 50 U/mL of IL-2 (Teceleukin; Roche, Nutley, NJ) and
137 5 μg/mL phytohemagglutinin (Roche, Basel, Switzerland) to generate T cell blasts [31]. The
138 study using blood from WHIM patients and healthy donors was approved by the
139 Institutional Review Board of the 12 de Octubre Health Research Institute (Nº CEIm:
140 24/248), and was conducted according to the principles of the Declaration of Helsinki.
141 Informed consent was obtained from all patients.

142 Recombinant gp120 protein, HXBc2, was obtained from MyBiosource (#MBS43404,
143 MyBiosource Inc., San Diego, CA). The following antibodies were used: anti-human
144 CXCR4 monoclonal antibody (mAb) (clone 44717) and phycoerythrin-conjugated anti-
145 human CXCR4 mAb (clone 12G5; both from R&D Systems, Minneapolis, MN); goat
146 F(ab')2 anti-mouse IgG-PE (Southern Biotech, Birmingham, AL); anti-human CD4 mAb
147 (clone OKT4; Biolegend, San Diego, CA); anti-histidine mAb (clone AD1.1.10; R&D
148 Systems); rabbit anti-$gp120_{IIIb}$ Ab [32]; rabbit anti-Gag p24 HIV-1 mAb (R&D Systems);
149 and anti-phospho-AKT mAb (S473; #4060), anti-phospho-ERK1,2 mAb (T202/Y204;
150 #9191) and anti-phospho-Lck mAb (Y505; #2751) (all from Cell Signaling Technology,
151 Danvers, MA); anti-tubulin mAb conjugated with rhodamine (Bio-Rad, Hercules, CA);
152 phalloidin-TRITC (#P1951, Sigma-Merck, St Louis, MO); anti-ICAM 3 mAb (clone
153 HP2/19) kindly donated by Dr. Francisco Sánchez Madrid; goat anti-mouse-AF488 Ab
154 (Thermo Fisher Scientific); anti-human gp120 mAb Fab fragments (clone 2G12;
155 Polymun Scientific, Vienna, Austria); anti-human IgG Fab fragments (Jackson
156 ImmunoResearch, West Grove, PA) conjugated to Abberior STAR RED (Abberior
157 GmbH, Gottingen, Germany) kindly donated by Dr. Jakub Chojnacki; anti- p24 HIV-1
158 (clone 37G12; Polymun Scientific, Vienna, Austria) conjugated with Abberior STAR
159 ORANGE. Human CXCL12 was obtained from PeproTech (Rocky Hill, NJ), and human
160 CXCR4 was cloned into the pAcGFPm-N1 plasmid (Clontech Laboratories, Palo Alto,
161 CA), as described [33].

162 Fab fragments for staining in stimulated emission depletion (STED) microscopy
163 were generated from the respective IgGs using the Fab Micro Preparation 3 Kit (Pierce,
164 Thermo Fisher Scientific). The quality of Fab preparations was determined by measuring
165 the absorbance of the eluted fractions of each conjugated antibody (at 280 nm and at the
166 wave-length of maximum absorption of the fluorochrome). Anti-human Fab fragments

167 were coupled to Abberior STAR RED dye *via* NHS-ester chemistry according to the dye
168 manufacturer's instructions.
169 CellTracker Orange CMTMR and Blue CMAC (#C2927 and #C2110,
170 respectively) were from Thermo Fisher Scientific.
171 ***Gene constructs***
172 Genes of HIV-1 gp120 (residues 31-507) from the isolate HXB2 (HIV-1_{IIIB}), with a C-
173 terminal 6×histidine tag, were amplified by PCR from pHXB2-env (#1069 NIH-AIDS
174 Reagent Program) using the oligonucleotides 5'NheI (5' TAACCGGTGCCAC
175 CATGGACAGAGCCAAGCTGCTGCTGTTGCTGCTGCTGCTGCTGCCTCAG
176 GCTCAGGCCACTGAGAAGCTGTGGGTG 3') and 3'NotI (5' ATGCGGCCGCTCA
177 GTGATGGTGATGGTGATGGGATCCACGCGGAACCAGCTGCACCACTCTTCT
178 3'), and were cloned into pIRES-PURO3 (#631619 from Clontech).
179 The CD4 extracellular domain (residues 1-388), with a C-terminal 6×histidine tag, was
180 amplified by PCR from CD4-pcDNA-3.1, kindly donated by Dr. Santos Mañes (Centro
181 Nacional de Biotecnología, CSIC) [34] using the oligonucleotides 5'AgeI (5'
182 TAACCGGTATGAACCGGGGAGTCCCT 3') and 3' NotI (5' ATGCGGCCGCCTAGTATG
183 GTGATGGTGATGCAAGTCCTCTTCAGAAATGAGCTTTTGCTCGGGCAGAACCT
184 TGAT 3'), and was cloned into pIRES-PURO3 (#631619 from Clontech).
185 Stably-transfected HEK-293T cell lines were generated for each construct. Briefly, 0.5 ×
186 10^6 cells were seeded in DMEM supplemented with 10% FCS in a 6-well plate 24 hours
187 before transfection. Cells were then transfected with Expifectamine in OptiMem media
188 (ExpiFectamine™ 293 transfection kit; #A14525 from Thermo Fisher Scientific). At 48
189 hours post-transfection, cells were transferred to DMEM containing 10% FBS and 2
190 μg/mL puromycin for selection (1 × 10^4 cells per well in a 96-well plate). Protein
191 expression was confirmed by western blot (using anti-gp120IIIB or anti-histidine mAbs,

192 depending on the construct). Positive clones were expanded, frozen, and stored in liquid
193 nitrogen.

194 ***Purification of recombinant proteins: soluble HIV-1 gp120 and soluble CD4***

195 HEK-293T cells expressing C-terminal his-tagged HXB2-gp120 or the extracellular CD4
196 domain were grown in DMEM containing 10% FBS and 2 μg/mL puromycin in 150-mm
197 plates. The filtered supernatants were passed through a Nickel Agarose Extrachel column,
198 Ni-NTA, (ABT technologies, UK) at a flow rate of 0.5 mL/min. Each recombinant
199 histidine-tagged protein was eluted utilizing a step-gradient protocol using a Tris 50 mM
200 pH 8, NaCl 500 mM buffer containing 500 mM imidazole. The elution involved initial
201 steps of 10 and 20% imidazole, followed by a linear gradient to 100% to ensure complete
202 protein recovery. The eluted fractions were analyzed by SDS-PAGE gel electrophoresis.
203 Those fractions containing the protein of interest were pooled and concentrated to a final
204 volume of 0.5 mL. The concentrated sample was subjected to gel filtration
205 chromatography using a S200 Increase (10/300) column (Cytiva, Freiburg, Germany).
206 The eluted fractions were analyzed by SDS-PAGE and fractions containing the expected
207 molecular size were pooled, aliquoted, and stored at -80ºC.

208 ***Production of viral-like particles and lentiviral particles***

209 Production of VLPs in HEK-293T cells included transfection with a plasmid encoding
210 the X4-tropic HIV-1 Env (10 μg pHXB2env; #1069 NIH-AIDS Reagent Program) and a
211 plasmid encoding a second-generation packaging system (7 μg psPAX2; #12260
212 Addgene). Supernatants were collected 48 hours post-transfection, filtered through 0.45
213 μm filters, and clarified by ultracentrifugation (247,000 × g, 2 h, 4°C) on a 20% sucrose
214 cushion, using a Beckman SW55 rotor. The resulting VLPs were aliquoted and stored at
215 -80°C. Expression of gp120 and p24 was assessed by western blotting with specific

216 antibodies. Each VLP batch was quantified using a p24 Quantikine ELISA kit (R&D
217 Systems).

218 Production of lentiviral particles (LVPs) was performed as above with the co-
219 transfection of a reporter gene (8 μg plGFP; #PS100065, OriGene, Rockville, MD)
220 instead of the double transfection. Supernatants were collected 48 hours post-transfection,
221 filtered through 0.45 μm filters, aliquoted, and stored at -80°C. Expression of gp120 and
222 p24 was assessed by western blotting with specific antibodies. Each LVP batch was
223 characterized in a transduction assay using LVPs transfected with the vesicular stomatitis
224 virus G glycoprotein (VSVG) (pCMV-VSV-G; #8454, Addgene) as a positive control.

225 ***Western blotting***

226 Cells (3×10^6) were activated with CXCL12 (50 nM) or recombinant X4-gp120 (0.3
227 μg/mL) at the time points indicated and then lysed in RIPA detergent buffer containing 1
228 mM PMSF, 10 μg/mL aprotinin, 10 μg/mL leupeptin, and 10 μM sodium orthovanadate
229 (30 min, 4ºC). Cell extracts were analyzed by western blotting using specific antibodies.
230 Densitometric evaluation of western blots was performed using ImageJ software (NIH,
231 Bethesda, MD).

232 ***Flow cytometry***

233 Cells (2×10^5/well) were incubated with specific antibodies (30 min, 4ºC) and mean
234 fluorescence intensity (MFI) was determined on a Gallios or FC500 flow cytometer
235 (Beckman Coulter). When required, Jurkat cells expressing CD4 ($JKCD4^+X4^+$ and
236 $JKCD4^+X4^-$) were incubated with X4-gp120-His (0.3 μg/mL), followed by staining with
237 an anti-histidine-PE mAb. Similarly, Daudi cells were incubated with a mixture of X4-
238 gp120 (0.3 μg/ml) and soluble hCD4-his (0.2 μg/mL), and subsequently stained with an
239 anti-histidine-PE mAb.

240 For human PBMCs, 100 μL of whole blood from healthy controls and a WHIM
241 patient were analyzed by flow cytometry for the expression of CD3-APC (IM2467),
242 CD19-PC5.5 (A66328), CD4-FITC (A07750), CD8-PC7 (737661; all from Beckman
243 Coulter Inc., Brea, CA), and CXCR4-PE (306506, Biolegend) using a Gallios flow
244 cytometer and FlowJo software.

245 Receptor internalization was evaluated after cell activation (5×10^5 cells/well)
246 with 50 nM CXCL12 or 0.3 μg/mL of recombinant X4-gp120 at the indicated time points.
247 Cells were incubated with an anti-CXCR4 mAb (clone 44717, 30 min, 4°C), followed by
248 a PE-coupled goat anti-mouse IgG (30 min, 4ºC) or, when required, with anti-CD4 (clone
249 OKT4, 20 min, 4ºC), and analyzed in a Cytoflex cytometer (Beckman Coulter). Results
250 are expressed as a percentage of mean spot intensity (MSI) of treated cells relative to that
251 of unstimulated cells.

252 To evaluate VLPs by flow cytometry, particles were coupled to latex beads (4
253 mm, 4% w/v Aldehyde/Sulfate latex; Invitrogen, Eugene, OR). After sonication (5 min,
254 RT), beads were mixed with VLPs at a ratio of 1:1 v/v (15 min, RT) in 1% casein-PBS
255 solution (Bio-Rad). Reactive groups were blocked with 100 mM glycine (60 min, 4°C,
256 with continuous rocking). Beads coupled to VLPs were washed twice by centrifugation
257 (3 min, 2000 × g) in washing buffer (PBS/BSA 0.5%), resuspended, and incubated with
258 the corresponding dilution of the recombinant soluble CD4 in casein-PBS solution (30
259 min, RT). VLP-beads conjugates were washed three times (3 min, 2,000 × g) with PBS
260 staining buffer (PBS supplemented with 2% FBS, 1% BSA, and 0.2% sodium azide) and
261 stained as above for flow cytometry.

262 ***Lentiviral particle transduction assays***

263 HEK-293 CD4 cells (1.2×10^4 cells per well in a 96-well plate) were inoculated with
264 serial dilutions of LVP-containing supernatants. Stock solutions were diluted in DMEM,

265 10% FCS, 1 mM pyruvate, and 2 mM glutamine. Sixteen hours later, the viral inoculum
266 was replaced with fresh medium and the cells were further incubated (48 h, 37°C). Viral
267 transduction efficiency was determined by GFP fluorescence analysis. The medium was
268 discarded and cells were washed with PBS and fixed using 4% formaldehyde in PBS (20
269 min, RT). Fluorescence was imaged in a Tecan Spark Cyto plate reader (Tecan Group
270 Ltd., Maenndorf, Switzerland) after extensive washes with PBS. Images of 2456 × 2052
271 pixels at a 16-bit gray scale were acquired with a 4× objective. All images were captured
272 using identical exposure settings (200 ms), except for wells where cells were transduced
273 with LVPs expressing VSVG, for which an exposure time of 80 ms was used. Mean
274 fluorescence intensity of GFP signal of each image was quantitated using Fiji/ImageJ
275 v2.3.0/1.53t software.

276 ***Cell-cell fusion assay***

277 The JKHXBC2 cell line was co-cultured with the indicated JK target cells at a 1:1 ratio
278 in 96-well flat-bottom plates (16 h, 37°C). Prior to co-culture, each cell type was stained
279 with vital probes CellTracker Orange CMTMR and Blue CMAC, respectively. Double-
280 stained events were subsequently analyzed using a Gallios Analyzer cytometer (Beckman
281 Coulter). Results are shown as the percentage of fusion events ± SD, using as a reference
282 the fusions events detected in JKCD4$^+$CXCR4$^+$ cells.

283 ***Cell adhesion/migration on planar lipid bilayers***

284 Planar lipid bilayers were prepared as reported [35]. Briefly, unlabeled GPI-linked
285 intercellular adhesion molecule 1 (ICAM-1) liposomes were mixed with 1,2-dioleoyl-
286 phosphatidylcoline. Membranes were assembled in FCS2 chambers (Bioptechs, Butler,
287 PA), blocked with PBS containing 2% FCS (60 min, RT), and coated with CXCL12 (200
288 nM, 30 min, RT) or gp120 (0.3 μg/ml, 30 min, RT). Cells (3 × 10^6 CD4$^+$ T blasts/mL) in
289 PBS containing 0.5% FCS, 0.5 g/L D-glucose, 2 mM $MgCl_2$, and 0.5 mM $CaCl_2$ were

290 then injected into the pre-warmed chamber (37ºC). Confocal fluorescence, differential
291 interference contrast (DIC) and interference reflection microscopy (IRM) images were
292 acquired on a Zeiss Axiovert LSM 510-META inverted microscope with a 40× oil-
293 immersion objective. Imaris 7.0 software (Bitplane, Zurich, Switzerland) and ImageJ
294 1.49v were used for qualitative and quantitative analysis of cell dynamics parameters,
295 fluorescence and IRM signals. The fluorescence signal of the planar bilayer in each case
296 was established as the background fluorescence intensity. The frequency of adhesion
297 (IRM^+ cells) per image field was estimated as [nº of cells showing IRM contact/total
298 number of cells (estimated by DIC)] × 100; similarly, we calculated the frequency

299 ***STED assays***

300 Purified particles (~1 μg of p24) were adhered to glass cover slips previously coated with
301 0.01% poly-L-lysine (Sigma) for 20 minutes. Cover slips were briefly fixed with 3%
302 PFA/PBS and blocked using 2% BSA (Sigma)/PBS for 30 minutes. Particles were stained
303 for Env using 10 ng/μL 2G12 Fab fragments and anti-human Abberior STAR RED-
304 conjugated Fab fragments. Following immunostaining, particles were washed in
305 permeabilization buffer (0.1% saponin, 0.5% BSA in PBS) and stained for Gag using 20
306 ng/μL 37G12 Ab conjugated with STAR ORANGE. The samples were briefly fixed using
307 3% PFA/PBS again and were overlaid with SlowFade Diamond (Thermo Fisher
308 Scientific). All steps were carried out at RT.

309 The VLPs were imaged using an Olympus IX83 inverted confocal microscope
310 equipped with the Abberior STEDYCON STED system using a 60×/1.42NA objective.
311 The following parameters were used during STED image acquisitions: pinhole size: 1
312 Airy; dwell time: 300 μs/pixel; field of view: 20 μm × 20 μm and pixel size: 20 nm.
313 The mature state of VLPs, the percentage which express gp120 on their surface and the
314 intensity of the signal of gp120 per VLP, were quantified manually using ImageJ.

315 ***Imaging of viral-like particles by transmission electron microscopy***

316 The integrity of VLPs was examined by negative-stain electron microscopy on carbon
317 grids. Samples were incubated on the grids and were treated with 2% uranyl acetate (30
318 s, RT). Grids were examined using a transmission electron microscope (1200-EX II; Jeol,
319 Tokyo, Japan) at 100 kV, equipped with a Gatan Oneview CMOS camera.

320 ***FRET saturation curves by sensitized emission***

321 FRET analyses were performed as described [36]. Briefly, HEK-293T cells (3.5×10^5
322 cells/well) were transiently transfected with cDNA encoding the fusion proteins using the
323 poly-ethylenimine method (Sigma-Aldrich). For CD4/CXCR4 or CD4/CXCR4^{R334X}
324 heterodimers, the cells were co-transfected with a fixed amount of CD4-CFP (2 μg) and
325 increasing amounts of CXCR4-YFP or CXCR4^{R334X}-YFP (0.5–8.0 μg). As a control, we
326 used a fixed amount of CD4-CFP (2 μg) and increasing amounts of 5HT$_{2B}$-YFP (0.5–12
327 μg). We incubated cells with cDNA and poly-ethylenimine (5.47 mM in nitrogen
328 residues) and 150 mM NaCl in serum-free medium, which was replaced after 4 hours by
329 complete medium. At 48 hours post transfection, cells were washed twice in HBSS
330 supplemented with 0.1% glucose and resuspended in the same solution. Total protein
331 concentration was determined for whole cells using the Bradford Assay Kit (Bio-Rad).
332 Cell suspensions (0.2 μg/μL) were added to black 96-well microplates and emission light
333 was quantified using the Wallac Envision 2104 Multilabel Reader (Perkin-Elmer,
334 Waltham, MA) as described [27]. To determine FRET$_{50}$ and FRET$_{max}$ values, curves were
335 extrapolated from data using a nonlinear regression equation applied to a single binding
336 site model with a 95% confidence interval (GraphPad PRISM software, San Diego, CA).
337 When FRET at a fixed ratio was needed, HEK-293T cells were transiently co-transfected
338 with a fixed ratio of CXCR4-YFP/CD4-CFP (15 μg and 9 μg, respectively) and
339 CXCR4^{R334X}-YFP/CD4-CFP (9 μg and 9 μg, respectively in all cases). After 48 hours the

340 cells were treated with empty VLPs (0.1 μg/mL of Gag p24) or gp120-VLPs (0.1 μg/mL
341 of Gag p24) and FRET efficiency was evaluated (n = 3, mean ± SD).

342 ***Single-molecule TIRF imaging and analysis***

343 Transfected cells expressing 8,500–22,000 receptors/cell (<4.5 particles/μm^2) were
344 selected for detection and tracking analysis. Experiments were performed at 37ºC with
345 5% CO_2 using a TIRF microscope (Leica AM TIRF inverted microscope; Leica
346 Microsystems, Wetzlar, Germany). Image sequences of individual particles (500 frames)
347 were then acquired at 49% laser power (488-nm diode laser) with a frame rate of 10 Hz
348 (100 ms/frame). The penetration depth of the evanescent field was 90 nm. Particles were
349 detected and tracked using the U-Track2 algorithm [37] implemented in MATLAB, as
350 described [27]. MSI, number of mobile and immobile particles and diffusion coefficients
351 (D_{1-4}) were calculated from the analysis of thousands of single trajectories over multiple
352 cells (statistics provided in the respective figure captions) using described routines [27]. The
353 receptor number along individual trajectories was determined as reported [38], using the
354 intensity of the monomeric protein CD86-AcGFP as a reference. Values were confirmed
355 using single-step photobleaching analysis.

356 ***HIV-1 infection in T CD4$^+$ cells of a WHIM patient***

357 All donors were female and under the age of 30. PBMCs were obtained from sero-
358 negative fresh blood of a WHIM patient and three healthy donors controls using SepMate
359 tubes (STEMCELL technologies, Vancouver, Canada). Isolated PBMCs were cultured in
360 RPMI supplemented with 20% FBS (Gibco), 1% penicillin/streptomycin (Capricorn
361 Scientific GmbH, Ebsdorfergrund, Germany), 3 μg/mL PHA (Sigma-Aldrich), and 10
362 U/mL of IL-2 (Novartis, Basel, Switzerland) for 48 hours at 37°C. Activated PBMCs
363 were inoculated *in vitro* at a multiplicity of infection (MOI) of 0.001 with the HIV-1 NL4-
364 3 lab strain for 1 hour. After removal of the viral inoculum, cultures were split into two

365 wells and maintained in RPMI supplemented with 20% FBS, 1% penicillin/streptomycin,
366 and 10 U/mL of IL-2. Supernatants were collected at different time points and replaced
367 with fresh supplemented media. The infection rate was determined by quantification of
368 viral p24 in the supernatants using the Alliance HIV-1 p24 Antigen Elisa Kit (Perkin
369 Elmer).

370 ***Statistical analyses***

371 All results were analyzed with GraphPad Prism software version 9. Cell polarization
372 assays, using immunofluorescence or planar lipid bilayers comparing different
373 conditions, were analyzed to determine significant differences between means using one-
374 way analysis of variance (ANOVA) followed by Tukey's multiple comparisons test. Data
375 related to the percentage of mature VLPs and their surface expression of gp120 obtained
376 by STED microscopy, and MFI results by flow cytometry, were also analyzed by one-
377 way ANOVA and Tukey's multiple comparisons test. A two-tailed Mann-Whitney non-
378 parametric test was used to analyze the MFI of gp120 per VLP. The Kruskal-Wallis test
379 followed by Dunn's test was used to analyze MSI and diffusion coefficients (D_{1-4}) of
380 single particles in TIRF experiments. We used contingency tables to compare two or more
381 groups of categorical variables, such as the percentages of mobile or immobile particles,
382 and these were compared using a Chi-square test with a two-tailed p-value. Statistical
383 differences were reported as n.s. = not significant $p > 0.05$, *$p \leq 0.05$, **$p \leq 0.01$, ***p
384 ≤ 0.001 and ****$p \leq 0.0001$.

385

386 **Results**

387 **Recombinant gp120-mediated CXCR4 clustering requires CD4 expression**

388 To evaluate the role of HIV-1 in modulating CXCR4 dynamics at the cell membrane, we
389 first synthesized a recombinant X4 HIV-1 gp120 (X4-gp120) with a C-terminal histidine
390 tag to facilitate subsequent detection. We generated a HEK-293T cell line that
391 constitutively secretes the recombinant glycoprotein. The secreted X4-gp120 was isolated
392 from cell culture supernatants using a simple, rapid, non-denaturing and efficient
393 purification procedure involving Ni-NTA agarose chromatography and gel filtration
394 chromatography. The purity of the isolated glycoprotein was confirmed by SDS-PAGE
395 and western blotting, using commercial gp120 as a control and specific antibodies
396 (Supplementary Figure 1A, B). The X4-gp120 specifically bound to Jurkat cells
397 expressing CD4, regardless of the presence or absence of CXCR4 (JKCD4^{+}CXCR4^{+} and
398 JKCD4^{+}CXCR4^{-}, respectively) (Supplementary Figure 1C). By contrast, X4-gp120 did
399 not bind to Daudi cells, which express only CXCR4 (Supplementary Figure 1D). In this
400 latter case, X4-gp120 binding became possible when the recombinant protein was pre-
401 incubated with soluble CD4 (Supplementary Figure 1D). These data indicate that our
402 recombinant gp120 is a X4-tropic gp120 capable of binding Jurkat cells expressing CD4.

403 Engagement of the HIV-1 Env with CD4 and/or a chemokine co-receptor activates
404 several signal transduction pathways [39,40]. For instance, gp120 binding to CD4 leads to
405 the phosphorylation of the receptor tyrosine kinase p56Lck, which then activates the
406 Raf/MEK/ERK and phosphatidylinositol 3-kinase (PI3K) pathways [41]. PI3K is also
407 activated through chemokine receptor engagement [42], and only viruses capable of
408 inducing signaling *via* these receptors can establish productive infections [40]. Jurkat cells
409 and primary CD4^{+} T blasts were stimulated with X4-gp120, then lysed and analyzed by
410 western blotting. The results showed that Akt, ERK1/2 and Lck were rapidly

411 phosphorylated following X4-gp120 activation (Supplementary Figure 2A,B) in both cell
412 types. Furthermore, it is known that the interaction of gp120 with CXCR4 influences the
413 actin cytoskeleton [43]. Cytochalesin D, an inhibitor of F-actin polymerization, has been
414 shown to inhibit viral entry into PBMCs [44] and to affect the formation of HIV-1 reverse
415 transcriptase products in HeLa cells [45]. We thus evaluated whether X4-gp120 reorganized
416 the actin cytoskeleton of the target cells. Using artificial lipid bilayers coated with ICAM-
417 1, we observed that both CXCL12 and X4-gp120 induced the polarization of primary
418 $CD4^+$ T blasts and, furthermore, enhanced cell adhesion (Supplementary Figure 3A, B).
419 However, only CXCL12 triggered significant cell migration (Supplementary Figure 3C).
420 These findings confirmed that X4-gp120 bound CXCR4 in the presence of CD4 and was
421 fully functional on both primary $CD4^+$ T blasts and Jurkat cells.

422 The actin cytoskeleton acts as a physical barrier, influencing the
423 compartmentalization of the plasma membrane and the dynamics of membrane proteins
424 [46,47]. Consequently, the dynamic nature of actin not only defines cell shape during
425 migration, but also affects membrane organization of both CD4 [48] and CXCR4 [27]. Next,
426 we transiently transfected $JKCD4^+X4^-$ cells, which express endogenous CD4, with
427 CXCR4-AcGFP. We then used SPT in TIRF-M mode to observe individual molecules
428 within the plasma membrane, allowing us to determine the effect of X4-gp120 on CXCR4
429 dynamics and stoichiometry (Supplementary video 1-3). Consistent with previous
430 observations [27,28], our analysis of CXCR4 dynamics in unstimulated cells revealed that
431 the majority of CXCR4 particles were mobile (~87%) (Figure 1A), exhibiting a median
432 short time-lag diffusion coefficient ($D_{1–4}$) of 0.017 $\mu m^2 s^{-1}$ (Figure 1B). Upon stimulation,
433 both CXCL12 and X4-gp120 significantly reduced the overall receptor diffusivity
434 (CXCL12, median $D_{1–4} = 0.007\ \mu m^2\ s^{-1}$; X4-gp120, median $D_{1–4} = 0.009\ \mu m^2\ s^{-1}$) (Figure
435 1B), and increased the percentage of immobile particles from ~13% (basal) to ~20%

436 (CXCL12), and to ∼18% (X4-gp120). To quantify the number of receptors in individual
437 trajectories, we measured the average fluorescence intensity during the initial 20 frames
438 of each trajectory and used the intensity of the monomeric protein CD86-AcGFP as a
439 reference value [28,49]. In unstimulated cells, we found a predominance of CXCR4
440 monomers and dimers (∼98%), with only a minor fraction of oligomers, complexes
441 containing more than three receptors (∼2%). Upon the addition of saturating X4-gp120
442 concentrations, we observed a significant reduction in the percentage of monomers and
443 dimers (∼82%) and a corresponding increase in nanoclusters composed of ≥3
444 receptors/particle (∼18%) (Figure 1C). This observation aligns with previous findings for
445 CXCL12 [27] As a control, stimulation with CXCL12 resulted in a larger percentage of
446 these nanoclusters (∼26%) (Figure 1C). These data correlated with the higher MSI values
447 observed after cell activation (basal 933 a.u.; CXCL12 2,105 a.u., X4-gp120 1,738 a.u.)
448 (Figure 1D). Collectively, these results indicate that X4-gp120 triggers CXCR4
449 nanoclustering, although to a lesser extent than CXCL12.

450 **gp120-expressing virus-like particles mediate CXCR4 clustering**

451 Recombinant X4-gp120 alone does not fully replicate the function of HIV-1 Env.
452 Previous studies have shown that the Env consists of gp120 trimers that redistribute and
453 cluster on the surface of virions following proteolytic Gag cleavage during maturation [50].
454 Considering the low number of Env trimers on natural HIV virions [51–53], this clustering is
455 crucial for establishing multiple receptor interactions necessary for virus entry. To mimic
456 the behavior of the virus, we prepared VLPs containing the X4 HIV-1 Env. HEK-293T
457 cells were transiently transfected with pHXB2env, psPAX2, and, when required, a
458 pLentiGFP plasmid that encodes a GFP reporter gene flanked by LTR regions. In this
459 latter case, we generated LVPs because these budding particles contained genetic material
460 and could transduce target cells. Supernatants were collected 48-hours post transfection,

461 and VLPs were purified by ultracentrifugation and resuspended in PBS. The structural
462 integrity of the VLPs was confirmed using negative-stain electron microscopy
463 (Supplementary Figure 4A). Western blot analysis of the samples, culture media, and
464 clarified supernatants confirmed the presence of both gp120 and p24 in VLPs and LVPs
465 (Supplementary Figure 4B). The gp120-containing viral particles bound soluble CD4
466 (Supplementary Figure 4C) and the corresponding LVPs successfully infected HEK-
467 293CD4 cells, as demonstrated in transduction assays (Supplementary Figure 4D). LVPs
468 containing VSVG were utilized as a positive control in these functional assays
469 (Supplementary Figure 4D).

470 Immature HIV-1 particles exhibit reduced entry efficiency [54,55]. This effect may
471 stem from the rigidity of the immature Gag lattice beneath the viral membrane, which
472 hinders membrane fusion [56] interactions between Gag and Env glycoproteins, limiting the
473 lateral mobility of the sparsely distributed Env trimers and, consequently, impairing the
474 clustering necessary for efficient infection [13]. Therefore, we evaluated the maturation
475 status of the generated VLPs using STED microscopy. We compared the condensation of
476 Gag and the distribution of Env molecules on the surface of the VLPs with those observed
477 on genetically immature particles and integrase-defective NL4-3ΔIN virions, serving as
478 controls [13]. Env proteins were stained with the human mAb 2G12, which specifically
479 recognizes the gp120 domain. To avoid antibody-induced clustering, we used purified
480 Fab fragments of 2G12. The location of individual HIV-1 particles was determined using
481 the human mAb 37G12, which targets the Gag protein and served as a "counterstain"
482 reference (Figure 2A). By assessing Gag condensation, we estimated that ~75% of the
483 VLPs, both gp120-VLPs and empty VLPs, were mature. These percentages were lower
484 for NL4-3ΔIN virions (~50%) and for immature VLPs (~16%) used as controls (Figure
485 2B). Furthermore, we observed that 26.5% of the gp120-VLPs, 40.2% of the NL4-3ΔIN

486 virions, and 40.5% of the immature VLPs expressed gp120. As a control, the anti-gp120
487 2G12 Fab did not stain particles lacking the Env (empty VLPs) (Figure 2A, C),
488 confirming the specificity of the staining. Moreover, STED analysis also revealed
489 differences in Env distribution between gp120-VLPs and NL4-3ΔIN virions, as
490 previously observed between mature and immature particles [13]. Specifically, gp120
491 staining intensity was higher for NL4-3ΔIN particles than for gp120-VLPs (NL4-3ΔIN
492 1,786 a.u. vs. gp120-VLPs 1,223 a.u.) (Figure 2D), suggesting a lower expression of Env
493 proteins in the latter. Analysis of gp120 intensity per particle demonstrated that g120-
494 VLPs had lower levels of gp120/particle than NL4-3ΔIN virions (Figure 2E). These data
495 confirmed the mature state of the gp120-VLPs generated and indicated that they
496 contained a reduced number of gp120/particle, similar to or even lower than that found
497 in primary HIV-1 viruses [53].

498 Next, we employed SPT-TIRF to investigate how gp120-VLPs affect CXCR4
499 dynamics in JKCD4^{+}X4^{-} cells that were transiently transfected with CXCR4-AcGFP
500 (Supplementary video 4-6). Analysis indicated that the gp120-VLPs significantly reduced
501 overall receptor diffusivity (basal, D_{1-4} = 0.025 μm^2 s^{-1}; VLPs, D_{1-4} = 0.017 μm^2 s^{-1};
502 gp120-VLPs D_{1-4} = 0.012 μm^2 s^{-1}) (Figure 3A). Under these conditions, we found
503 predominantly CXCR4 monomers and dimers at steady-state, and their proportion
504 decreased upon VLP treatment (basal ~99%; VLPs ~91%; gp120-VLPs ~71%).
505 Consequently, the percentage of nanoclusters containing ≥3 receptors/particle increased
506 (~1%, basal; ~9%, VLPs; ~29%, gp120-VLPs) (Figure 3B). These findings were
507 consistent with the MSI values (basal 761 a.u.; VLPs 1,150 a.u.; gp120-VLPs 1,898 a.u.)
508 (Figure 3C). While further research is necessary to elucidate the precise mechanism, the
509 effect induced by the empty VLPs suggests that, beyond the role of gp120 in promoting
510 conformational changes on CD4 and CXCR4, non-specific interactions between the viral

511 particles and the cell membrane might also influence the conformations of these two
512 receptors.

513 Our results indicated that, similar to the effect triggered by soluble X4-gp120,
514 VLPs containing HIV-1 Env also triggered CXCR4 nanoclustering. To understand the
515 role of CXCR4 clustering in HIV-1 infection, we next analyzed the behavior of the
516 WHIM mutant CXCR4, $CXCR4^{R334X}$, which does not oligomerize in the presence of
517 CXCL12 [28]. SPT-TIRF-M analysis of $JKCD4^{+}X4^{-}$ cells transiently transfected with
518 $CXCR4^{R334X}$-AcGFP (Supplementary video 7-9) demonstrated that, unlike the effect
519 described for CXCL12, the VLPs containing gp120 triggered $CXCR4^{R334X}$
520 oligomerization (basal MSI 669 a.u.; VLPs MSI 909 a.u.; gp120-VLPs MSI 1,730 a.u.)
521 (Figure 4A) and promoted a significant reduction in overall receptor diffusivity (basal,
522 median D_{1-4} = 0.021 $\mu m^2 s^{-1}$; gp120-VLPs, median D_{1-4} = 0.014 $\mu m^2 s^{-1}$) (Figure 4B).
523 Furthermore, gp120-VLP binding reduced the percentage of $CXCR4^{R334X}$ monomers and
524 dimers (steady-state ~99%; gp120-VLPs ~80%), while concurrently increasing the
525 percentage of nanoclusters containing ≥3 receptors/particle (basal ~1%; gp120-VLPs
526 ~20%) (Figure 4C).

527 In sum, these data indicate that whereas CXCL12 modulates CXCR4 dynamics
528 and clustering at the cell membrane, but not mutant $CXCR4^{R334X}$, the gp120 VLPs
529 similarly influence the behavior of both CXCR4 and $CXCR4^{R334X}$. This implies that
530 CXCL12 and gp120 binding stabilizes distinct conformational states of CXCR4.

531 **CD4 expression alters the conformation adopted by CXCR4**

532 Our results support a model where CXCL12 binds to either CXCR4 or $CXCR4^{R334X}$ [28].
533 By contrast, X4-gp120, whether alone or within the viral context, associates these co-
534 receptors when they are complexed with CD4. It is known that CD4/CXCR4 complexes

535 might facilitate co-operative interactions with HIV-1 during viral adsorption and/or entry
536 into human leukocytes [57].

537 To confirm the interaction between CD4 and CXCR4 [22] and to assess whether
538 $CXCR4^{R334X}$ could also interact with CD4, we conducted FRET analyses. Our results
539 demonstrated positive FRET signals for both complexes: CD4/CXCR4 ($FRET_{50}$=2.71)
540 and CD4/$CXCR4^{R334X}$ ($FRET_{50}$=0.40) (Figure 5A, B). As a control, we observed minimal
541 residual energy transfer in cells co-transfected with CD4-CFP and $5HT_{2B}$-YFP (Figure
542 5C). The presence of CD4/CXCR4 and CD4/$CXCR4^{R334X}$ heterodimers was also
543 investigated *in silico* using alphaFold3 [58] (Supplementary Figure 5). We focused on the
544 interaction between the transmembrane and intracellular fragments of CD4 and both
545 CXCR4 and $CXCR4^{R334X}$. The predicted template modeling (pTM) scores for both
546 complexes were close to 0.7, suggesting a reliable prediction of these interactions. The
547 modeling also indicated a preferred association of CD4 with CXCR4 between
548 transmembrane helices IV and V, although further analysis is needed to precisely
549 determine the interaction site. These data align with previous reports demonstrating a
550 constitutive association between CD4 and CXCR4 that can influence HIV-1 infection
551 [22,59–62] and our results extend this observation to the naturally occurring $CXCR4^{R334X}$
552 mutant. Furthermore, we observed increased FRET efficiency in both CD4-CXCR4 and
553 CD4-$CXCR4^{R334X}$ complexes upon gp120-VLPs binding (Figure 5D, E), confirming that
554 the VLPs induce conformational changes in these heterodimers.

555 Productive HIV-1 infection of $CD4^+$ cells markedly diminishes cell-surface
556 expression of CD4 [63,64]. However, the impact on chemokine receptors is less clear. While
557 some studies report a complete loss of CCR5 surface staining on cells chronically infected
558 with R5 viruses [65] the effect on CXCR4 varies [65,66]. Using flow cytometry, we
559 investigated how stimulation with X4-gp120 affects the cell-surface expression of CD4,

560 CXCR4, and CXCR4^{R334X}. Consistent with previous findings[67] , CXCL12 induced rapid
561 internalization of CXCR4 without altering CXCR4^{R334X} levels at the cell surface. By
562 contrast, X4-gp120 caused a gradual, slight decrease in the surface expression of both
563 receptors. Furthermore, CXCL12 did not affect CD4 surface levels, whereas X4-gp120
564 induced a gradual decline in CD4 expression (Figure 6A, B).

565 Taken together, our FRET and internalization experiments suggest that the effects
566 of X4-gp120 on CXCR4 and CXCR4^{R334X} differ from those of CXCL12 and are
567 dependent on their interaction with CD4.

568 Next, we investigated whether CD4/CXCR4^{R334X} complexes could also support
569 primary HIV-1 infection. Flow cytometry analysis showed no significant difference in
570 the ability of Jurkat cells expressing either CXCR4 or CXCR4^{R334X} to bind X4-gp120
571 (Figure 7A). In agreement, *in vitro* fusion assays using cells expressing CD4/CXCR4 or
572 CD4/CXCR4^{R334X}, and target cells expressing HIV pHXB2 Env, demonstrated a
573 significant increase in fusion events and syncytium formation in both Jurkat cell types
574 (Figure 7B, C). We then tested whether PBMCs isolated from a WHIM patient and
575 healthy donors were equally susceptible to infection by a primary X4 HIV-1_{NL4-3} viral
576 strain. We first analyzed the expression of CD4, and CXCR4 or CXCR4^{R334X} on these
577 PBMC samples by flow cytometry (Supplementary Figure 6A-C). Subsequently, cells
578 were stimulated with PHA and IL-2, and 48 hours later, inoculated with a primary X4
579 HIV-1_{NL4-3} virus at a MOI of 0.001 for 120 minutes. ELISA measurements of p24 levels
580 in the culture medium at various time points revealed similar viral infection rates in both
581 Healthy and WHIM PBMCs (Figure 7D).

582 Collectively, these data indicate that T cells from a WHIM patient exhibit similar
583 infection and viral replication rates with those isolated from healthy donors. Furthermore,
584 these data suggest that HIV-1 might modulate the conformation adopted by CXCR4 at

585 the cell membrane, which is associated with HIV-1 infection. The CXCR4 conformation
586 stabilized by HIV-1 binding likely differs from that induced by CXCL12 binding and
587 therefore supports a direct effect of the interactions with CD4 in establishing a permissive
588 conformation of CXCR4 for HIV-1 infection.

589 **Discussion**

590 The process of HIV-1 infection begins with the binding of the trimeric HIV-1 Env
591 glycoprotein to the CD4 receptor on the target cell surface [68–70]. Research suggests that
592 when the viral and cellular membranes are distant, the HIV-1 Env trimers initially engage
593 only one CD4 molecule, and as the Env moves closer to the membrane and adopts an
594 open conformation it gains the ability to bind a second and a third CD4 molecule [24]. CD4
595 binding thus induces conformational changes within the gp120 subunit of Env that enable
596 subsequent engagement of the co-receptors CCR5 or CXCR4. Receptor and co-receptor
597 engagement trigger further conformational changes in the Env gp41 subunits, ultimately
598 mediating the fusion of the viral and host cell membranes.

599 Competitive receptor inhibitors, such as soluble synthetic CD4 (sCD4), synthetic
600 CD4 peptides, and anti-CD4 binding site antibodies have been shown to block infection
601 both *in vitro* [71,72] and *in vivo* [73,74]. Notably, virus-like nanoparticles displaying clustered
602 membrane-associated CD4 were significantly more effective at blocking infection than
603 sCD4, CD4-Ig, or the broadly neutralizing monoclonal antibody 3BNC117 [75]. These
604 findings collectively suggest that the virus may induce CD4 clustering to promote cell
605 infection. Consistent with this idea, single-molecule super-resolution imaging revealed
606 that CD4 molecules on the cell membrane are predominantly found as individual
607 molecules or small clusters of up to 4 molecules, and that the size and number of these
608 clusters increase upon virus binding or gp120 activation [19]. These data therefore support
609 a model where viral binding triggers a nanoscale reorganization of CD4 on the plasma

610 membrane, a process necessary for cell infection. This observation aligns with substantial
611 evidence indicating that various cell-surface receptors are organized into clusters [23,76]. For
612 instance, T-cell receptors on T cells coalesce into nanoclusters within and around immune
613 synapses prior to signal transduction [77,78]. Receptor clustering has been also demonstrated
614 for numerous other transmembrane receptors, such as neurotransmitter receptors [79] and
615 immune receptors [80,81]. Furthermore, studies analyzing receptor dynamics during cell
616 movement using SPT have shown that chemokine-mediated receptor clustering is
617 essential for cells to accurately sense chemoattractant gradients [27,28].

618 Here, using SPT-TIRF-M analysis on Jurkat cells, we found that both recombinant
619 X4-gp120 and VLPs displaying X4 HIV-1 Env (with fewer gp120 molecules) promote
620 CXCR4 clustering and modify its dynamics in a CD4-dependent manner. Our data show
621 that, similar to the effect of CXCL12, gp120 binding to CXCR4 leads to a significant
622 decrease in the number of monomers and dimers, while increasing the proportion of
623 larger, generally immobile nanoclusters. Previous studies using immunoelectron
624 microscopy suggested that CCR5, CXCR4, and CD4 are mainly located on microvilli and
625 tend to form distinct, uniform microclusters in all cell types examined [57]. This clustering
626 is thought to enhance co-operative interactions with HIV-1 during virus adsorption and
627 entry into human leukocytes [57]. Single-molecule force spectroscopy has also revealed that
628 the force needed to break apart the gp120/CCR5/CD4 complex and its duration are greater
629 than those for the gp120/CD4 bond [82]. The formation of CCR5/CD4/CXCR4 oligomers
630 is implicated in the reduced infectivity of X4 HIV-1 in cells that also express CCR5 [22].

631 The data suggest that exposure to HIV-1 triggers several rearrangements of cell
632 receptors, highlighting the significance of these changes in facilitating viral entry into
633 target cells. Ligands of GPCRs promote the association of cytoplasmic signaling
634 molecules to the receptor, which contributes to reducing the diffusion rates of receptor

635 complexes and their ability to move within confined areas [83,84]. Receptor clustering, a
636 process known to enhance cell sensitivity [85], also promotes efficient cell signal
637 transmission [86] and increases the robustness of signaling systems [87]. Indeed, it is well
638 established that HIV-1 promotes CD4- and CXCR4-mediated signaling events that
639 facilitate viral entry and infection of host cells [39,88–91]. We observed that gp120 triggered
640 the phosphorylation of Lck, Akt and ERK1/2 and promoted cell polarization, although
641 this latter effect was less pronounced than that induced by CXCL12. Furthermore, in lipid
642 bilayer assays using ICAM-1 as a substrate, gp120 mediated Jurkat cell adhesion but did
643 not significantly promote cell migration compared with CXCL12. While soluble gp120
644 has been used to investigate certain HIV-1 effects on cells [39,43,92], employing saturating
645 concentrations of the glycoprotein might lead to non-specific effects on the dynamics of
646 receptors and co-receptors at the cell membrane. Moreover, the conformation of
647 recombinant gp120 may not accurately reflect its physiological structure on intact HIV-1
648 particles. Within virions, the Env glycoprotein complex forms a spike composed of a
649 heterotrimeric gp120 non-covalently associated with three gp41 molecules. Each virion
650 expresses between 7 and 14 such spikes, which, following maturation, reorganize into a
651 few large clusters that interact with cell receptors [13,51]. To address these limitations, we
652 generated VLPs displaying the X4 HIV-1 Env. Super-resolution microscopy confirmed
653 the maturity of the gp120-VLPs, expressing a very low number of gp120 trimers on their
654 surface, even fewer than the 7 to 14 Env trimers per virus particle previously reported on
655 primary isolated virions [52,93,94]. Similar to soluble recombinant gp120, these VLPs also
656 induced CXCR4 clustering and altered receptor dynamics. These findings thus confirm
657 that the effects observed with X4-gp120 are not artifacts resulting from the conformation
658 of the soluble gp120 or to the use of saturating concentrations. Receptor clustering was
659 initiated through binding of gp120-VLPs to CD4 and CXCR4, as neither X4-gp120 nor

660 the VLPs associated with CXCR4 in the absence of CD4. We confirmed this using a
661 mutant CXCR4, CXCR4^{R334X}, which does not oligomerize in the presence of CXCL12
662 [28]. CXCR4^{R334X} is found in cells of patients with WHIM syndrome, a rare combined
663 immunodeficiency characterized by the presence of warts, hypogammaglobulinemia,
664 recurrent bacterial infections and myelokathexis symptoms [29]. In these patients, the
665 inability of CXCL12 to induce receptor oligomerization leads to defects in actin
666 dynamics, preventing proper sensing of chemoattractant gradients [28,95]. We investigated
667 how VLPs containing the X4 HIV-1 Env affected the dynamics of CXCR4^{R334X} in cells
668 expressing CD4. Surprisingly, the X4 HIV-1 Env caused a significant reduction in
669 CXCR4^{R334X} monomers and dimers, while increasing the proportion of larger
670 nanoclusters, which were generally immobile. These findings suggest that CXCL12 and
671 gp120 VLPs have different effects on chemokine receptor dynamics, leading us to
672 hypothesize that the structure of CXCR4, whether or not it is associated with CD4, could
673 explain these observations. AlphaFold predictions and FRET analysis confirmed the
674 formation of CD4/CXCR4 complexes [22] and supported the existence of
675 CD4/CXCR4^{R334X} heterodimers. In both cases, gp120-VLPs binding altered the
676 conformations. These findings correlate with the syncytia formation observed in *in vitro*
677 fusion experiments between cells expressing the X4 HIV-1 Env and target cells
678 expressing either CD4/CXCR4 or CD4/CXCR4^{R334X}, and with the infection of PBMCs
679 from both WHIM patients and healthy donors when incubated with primary X4-HIV-1.
680 These findings also indicate that WHIM mutations do not protect against HIV-1 infection,
681 consistent with a previous *in vitro* study showing that CD4^{+}U87 cells expressing
682 CXCR4^{R334X} or CXCR4 are equally susceptible to a luciferase-expressing pseudotyped
683 virus infection [96]. In our experiments, we use fully replication-competent viruses rather
684 than pseudotyped viruses, and we study the dynamics of replication over a 7-day period,

685 rather than just a 24-hour snapshot. Beyond inducing CXCR4 aggregation, we observed
686 that X4-gp120 promoted the internalization of CD4 and CXCR4 and, surprisingly, also
687 triggered the internalization of $CXCR4^{R334X}$. This mutant receptor cannot internalize in
688 response to CXCL12 because it lacks the last 19 C-terminal amino acids, which are
689 necessary for GRK-mediated Ser/Thr phosphorylation and β-arrestin recruitment [29,97].
690 Some studies suggest that HIV-1 glycoproteins can reduce CD4 and CXCR4 levels during
691 HIV-1 entry [66,98,99], proposing receptor-mediated endocytosis as an alternative HIV-1
692 entry mechanism [100–105]. HIV-1-mediated endocytosis also explains the reduction of CD4
693 and $CXCR4^{R334X}$ at the cell membrane and the similar infection rates in PBMCs from
694 WHIM patients and healthy donors. Although direct evidence for the internalization of
695 CD4 and CXCR4 as complexes is lacking, their co-localization in lipid rafts during HIV-
696 1 [32,106,107] and their ability to form heterocomplexes [22] strongly suggest they could be
697 endocytosed together. Therefore, we hypothesize that gp120 binding to CD4 stabilizes
698 CD4/CXCR4 complexes, and that the conformation of CXCR4 within these complexes
699 might differ from that of CXCR4 homodimers.

700 We also detected a residual but significant effect of empty VLPs on the dynamics
701 of both CXCR4 and of $CXCR4^{R334X}$. This is likely not receptor-mediated, as these control
702 VLPs lacked the X4 HIV-1 Env. While further experiments are needed, a potential
703 interaction between the lipids and or cell adhesion molecules derived from the cells where
704 the virions were produced, and those in the cell membrane could explain this observation.
705 It is well established that the lipid composition of the cell membrane influences ligand-
706 mediated chemokine receptor oligomerization and dynamics [108,109]. Additionally,
707 glycosaminoglycans, such as heparin and heparan sulphate, might play a role in the
708 attachment of virions to various cell types [110–112]. Although their effects on R5 strains are

709 debated [113–115], the concentrations of these glycosaminoglycans vary considerably
710 between cells [116].

711 Our data indicate that HIV-1 not only affects CD4 dynamics, which is well known,
712 but also alters the spatial distribution and dynamics of CXCR4 in a manner distinct from
713 the effects of its natural ligand, CXCL12. While HIV-1 binding involves CD4/CXCR4
714 complexes, CXCL12 binds exclusively to CXCR4, potentially leading to different effects
715 on CXCR4 conformations. These findings might also explain why HIV-1 induced the
716 endocytosis of both CD4/CXCR4 and CD4/CXCR4^{R334X} complexes, whereas CXCL12
717 did not mediate the internalization of either CD4 or the CD4/CXCR4^{R334X} complex. This
718 suggests that the interaction of both co-receptors with CD4 may result in different
719 conformations of CXCR4 and CXCR4^{R334X} compared with their respective homodimers.
720 The interaction motif between CD4 and CXCR4 should be considered a crucial target for
721 disrupting complex dynamics at the cell membrane, potentially opening new avenues for
722 anti-HIV-1 therapies.

723 **Acknowledgements**

724 This work was supported by grants from the Spanish Ministry of Science and Innovation
725 (PID2020-114980RB-I00 and PID2023-146301OB-I00) to MM and (PID2022-
726 140651NB-I00) to CS, and (PID2022-139271OB-I00 and CB21/13/00063) to JM-P. EG-
727 C and BS were supported by the program Apoyos Centros de Excelencia S.O. of the
728 Spanish Ministry of Science and Innovation (SEV-2017-0712). AQ-F and SRG ere
729 included in the doctoral program of the Department of Molecular Biosciences and of
730 Biology, respectively, Universidad Autónoma de Madrid, and are supported by the Fondo
731 de Personal Investigador (FPI) program of the Spanish Ministry for Science and
732 Innovation (PRE2018-083201 and PRE2019-087966, respectively). EAB is included in
733 the doctoral program of Biomedicine, University of Barcelona, and is supported by the

FPI program of the Spanish Ministry for Science and Innovation (PRE2022-000847). RA-B is supported by the Garantía Juvenil program of the Regional Government of Madrid, Spain (CAM20_CNB_AI_07). LIGG receives funding from Institute of Health, Carlos III co-funded by Fondos FEDER Project FIS PI21/01642.We also acknowledge the technical help of the Advance Light Microscopy Unit at the CNB/CSIC.

JMP has received research funding, consultancy fees, and lecture sponsorships from and has served on advisory boards for various companies (AbiVax, AstraZeneca, MSD, Gilead Sciences, ViiV Healthcare, Johnson & Johnson) outside the scope of this article. The rest of the authors declare no competing interests.

Author Contributions

J.M.R.-F. and M.M. conceptualized the project and designed all aspects of the study; A.Q.-F. and C.A.S. generated, purified and tested the functionality of X4-gp120; A.Q-F., E.S.S. and U.G. generated and tested the function of VLPs and LVPs; C.A.S. performed the analysis using Alphafold3; A.Q-F., E.M.G.-C., R.A.-B., S.R.G. and R.Villares, performed experiments; B.S.-P. developed the FRET assays; A.Q-F., E.M.G.-C., and J.M.R.-F. quantified the TIRFM images; and made the statistics; L.I.G.-G. was responsible of the ethycal permissions and provided blood samples from donors; A.Q.-F. and J.C developed the microscopy analysis of VLP maturation; E.A.-B., M.C.P. and J.M.-P. developed the infection experiments with primary viruses; A.Q.-F., C.A.S., J.M.R.-F., J.C., J.M.-P. and M.M. provided input into the Project. J.M.R.-F. generated all the figures, J.M.R.-F., C.S., J.C., J.M.-P and M.M. wrote the manuscript.

Bibliography

1. Kowalski, M. *et al.* Functional regions of the envelope glycoprotein of human immunodeficiency virus type 1. *Science* **237**, 1351–1355 (1987).
2. Lu, M., Blacklow, S. C. & Kim, P. S. A trimeric structural domain of the HIV-1 transmembrane glycoprotein. *Nature Structural Biology 1995 2:12* **2**, 1075–1082 (1995).

762 3. Choe, H. *et al.* The beta-chemokine receptors CCR3 and CCR5 facilitate infection
763 by primary HIV-1 isolates. *Cell* **85**, 1135–1148 (1996).
764 4. Feng, Y., Broder, C. C., Kennedy, P. E. & Berger, E. A. HIV-1 entry cofactor:
765 functional cDNA cloning of a seven-transmembrane, G protein-coupled receptor.
766 *Science* **272**, 872–877 (1996).
767 5. Wolinsky, S. M. *et al.* Adaptive evolution of human immunodeficiency virus-type
768 1 during the natural course of infection. *Science* **272**, 537–542 (1996).
769 6. Lu, Z. H. *et al.* Evolution of HIV-1 coreceptor usage through interactions with
770 distinct CCR5 and CXCR4 domains. *Proc Natl Acad Sci U S A* **94**, 6426–6431
771 (1997).
772 7. Connor, R. I., Mohri, H., Cao, Y. & Ho, D. D. Increased viral burden and
773 cytopathicity correlate temporally with CD4+ T-lymphocyte decline and clinical
774 progression in human immunodeficiency virus type 1-infected individuals. *J Virol*
775 **67**, 1772–1777 (1993).
776 8. Carter, C. C. *et al.* HIV-1 Utilizes the CXCR4 Chemokine Receptor to Infect
777 Multipotent Hematopoietic Stem and Progenitor Cells. *Cell Host Microbe* **9**, 223–
778 234 (2011).
779 9. Landau, N. R., Warton, M. & Littman, D. R. The envelope glycoprotein of the
780 human immunodeficiency virus binds to the immunoglobulin-like domain of CD4.
781 *Nature* **334**, 159–162 (1988).
782 10. Arthos, J. *et al.* Identification of the residues in human CD4 critical for the binding
783 of HIV. *Cell* **57**, 469–481 (1989).
784 11. Zhang, W. *et al.* Conformational changes of gp120 in epitopes near the CCR5
785 binding site are induced by CD4 and a CD4 miniprotein mimetic. *Biochemistry* **38**,
786 9405–9416 (1999).
787 12. Doms, R. W. & Moore, J. P. HIV-1 membrane fusion: targets of opportunity. *J*
788 *Cell Biol* **151**, (2000).
789 13. Chojnacki, J. *et al.* Maturation-dependent HIV-1 surface protein redistribution
790 revealed by fluorescence nanoscopy. *Science* **338**, 524–528 (2012).
791 14. Buzon, V. *et al.* Crystal structure of HIV-1 gp41 including both fusion peptide and
792 membrane proximal external regions. *PLoS Pathog* **6**, 1–7 (2010).
793 15. Pancera, M. *et al.* Structure of HIV-1 gp120 with gp41-interactive region reveals
794 layered envelope architecture and basis of conformational mobility. *Proc Natl*
795 *Acad Sci U S A* **107**, 1166–1171 (2010).
796 16. Garg, H., Viard, M., Jacobs, A. & Blumenthal, R. Targeting HIV-1 gp41-induced
797 fusion and pathogenesis for anti-viral therapy. *Curr Top Med Chem* **11**, 2947–2958
798 (2011).
799 17. Barrero-Villar, M. *et al.* Moesin is required for HIV-1-induced CD4-CXCR4
800 interaction, F-actin redistribution, membrane fusion and viral infection in
801 lymphocytes. *J Cell Sci* **122**, 103–113 (2009).
802 18. Jiménez-Baranda, S. *et al.* Filamin-A regulates actin-dependent clustering of HIV
803 receptors. *Nat Cell Biol* **9**, 838–846 (2007).
804 19. Yuan, Y. *et al.* Single-Molecule Super-Resolution Imaging of T-Cell Plasma
805 Membrane CD4 Redistribution upon HIV-1 Binding. *Viruses* **13**, (2021).
806 20. Lapham, C. K. *et al.* Evidence for cell-surface association between fusin and the
807 CD4-gp120 complex in human cell lines. *Science* **274**, 602–605 (1996).
808 21. Ugolini,', S. *et al.* HIV-1 gp120 Induces an Association Between CD4 and the
809 Chemokine Receptor CXCR4'. *The Journal of Immunology* **159**, 3000–3008
810 (1997).

22. Martínez-Muñoz, L. *et al.* CCR5/CD4/CXCR4 oligomerization prevents HIV-1 gp120IIIB binding to the cell surface. *Proc Natl Acad Sci U S A* **111**, (2014).
23. Hartman, N. C. & Groves, J. T. Signaling clusters in the cell membrane. *Curr Opin Cell Biol* **23**, 370–376 (2011).
24. Li, W. *et al.* HIV-1 Env trimers asymmetrically engage CD4 receptors in membranes. *Nature* **623**, 1026–1033 (2023).
25. Krummel, M. F., Sjaastad, M. D., Wulfing, C. W. & Davis, M. M. Differential clustering of CD4 and CD3zeta during T cell recognition. *Science* **289**, 1349–1352 (2000).
26. Kao, H., Lin, J., Littman, D. R., Shaw, A. S. & Allen, P. M. Regulated movement of CD4 in and out of the immunological synapse. *J Immunol* **181**, 8248–8257 (2008).
27. Martínez-Muñoz, L. *et al.* Separating Actin-Dependent Chemokine Receptor Nanoclustering from Dimerization Indicates a Role for Clustering in CXCR4 Signaling and Function. *Mol Cell* **70**, 106-119.e10 (2018).
28. García-Cuesta, E. M. *et al.* Altered CXCR4 dynamics at the cell membrane impairs directed cell migration in WHIM syndrome patients. *Proc Natl Acad Sci U S A* **119**, (2022).
29. Liu, Q. *et al.* WHIM syndrome caused by a single amino acid substitution in the carboxy-tail of chemokine receptor CXCR4. *Blood* **120**, 181–189 (2012).
30. García-Cuesta, E. M. *et al.* Altered CXCR4 dynamics at the cell membrane impairs directed cell migration in WHIM syndrome patients. *Proc Natl Acad Sci U S A* **119**, (2022).
31. Gardeta, S. R. *et al.* Sphingomyelin Depletion Inhibits CXCR4 Dynamics and CXCL12-Mediated Directed Cell Migration in Human T Cells. *Front Immunol* **13**, (2022).
32. Mañes, S. *et al.* Membrane raft microdomains mediate lateral assemblies required for HIV-1 infection. *EMBO Rep* **1**, 190–196 (2000).
33. Martínez-Muñoz, L. *et al.* Separating Actin-Dependent Chemokine Receptor Nanoclustering from Dimerization Indicates a Role for Clustering in CXCR4 Signaling and Function. *Mol Cell* **70**, 106-119.e10 (2018).
34. Del Real, G. *et al.* Blocking of HIV-1 infection by targeting CD4 to nonraft membrane domains. *J Exp Med* **196**, 293–301 (2002).
35. Carrasco, Y. R., Fleire, S. J., Cameron, T., Dustin, M. L. & Batista, F. D. LFA-1/ICAM-1 interaction lowers the threshold of B cell activation by facilitating B cell adhesion and synapse formation. *Immunity* **20**, 589–599 (2004).
36. Martínez Muñoz, L. *et al.* Dynamic regulation of CXCR1 and CXCR2 homo- and heterodimers. *J Immunol* **183**, 7337–7346 (2009).
37. Jaqaman, K. *et al.* Robust single-particle tracking in live-cell time-lapse sequences. *Nat Methods* **5**, 695–702 (2008).
38. Dorsch, S., Klotz, K. N., Engelhardt, S., Lohse, M. J. & Bünemann, M. Analysis of receptor oligomerization by FRAP microscopy. *Nat Methods* **6**, 225–230 (2009).
39. Balabanian, K. *et al.* CXCR4-Tropic HIV-1 Envelope Glycoprotein Functions as a Viral Chemokine in Unstimulated Primary CD4 + T Lymphocyteskk. *The Journal of Immunology* **173**, 7150–7160 (2004).
40. Arthos, J. *et al.* CCR5 signal transduction in macrophages by human immunodeficiency virus and simian immunodeficiency virus envelopes. *J Virol* **74**, 6418–6424 (2000).

860 41. Briand, G., Barbeau, B. & Tremblay, M. Binding of HIV-1 to its receptor induces
861 tyrosine phosphorylation of several CD4-associated proteins, including the
862 phosphatidylinositol 3-kinase. *Virology* **228**, 171–179 (1997).
863 42. Curnock, A. P., Logan, M. K. & Ward, S. G. Chemokine signalling: pivoting
864 around multiple phosphoinositide 3-kinases. *Immunology* **105**, 125–136 (2002).
865 43. Yoder, A. *et al.* HIV Envelope-CXCR4 Signaling Activates Cofilin to Overcome
866 Cortical Actin Restriction in Resting CD4 T Cells. *Cell* **134**, 782–792 (2008).
867 44. Iyengar, S., Hildreth, J. E. K. & Schwartz, D. H. Actin-dependent receptor
868 colocalization required for human immunodeficiency virus entry into host cells. *J*
869 *Virol* **72**, 5251–5255 (1998).
870 45. Bukrinskaya, A. G. HIV-1 assembly and maturation. *Arch Virol* **149**, 1067–1082
871 (2004).
872 46. Plowman, S. J., Muncke, C., Parton, R. G. & Hancock, J. F. H-ras, K-ras, and inner
873 plasma membrane raft proteins operate in nanoclusters with differential
874 dependence on the actin cytoskeleton. *Proc Natl Acad Sci U S A* **102**, 15500–15505
875 (2005).
876 47. Torreno-Pina, J. A. *et al.* The actin cytoskeleton modulates the activation of iNKT
877 cells by segregating CD1d nanoclusters on antigen-presenting cells. *Proc Natl*
878 *Acad Sci U S A* **113**, E772–E781 (2016).
879 48. Pereira, P. M. *et al.* Fix Your Membrane Receptor Imaging: Actin Cytoskeleton
880 and CD4 Membrane Organization Disruption by Chemical Fixation. *Front*
881 *Immunol* **10**, (2019).
882 49. Calebiro, D. *et al.* Single-molecule analysis of fluorescently labeled G-protein-
883 coupled receptors reveals complexes with distinct dynamics and organization.
884 *Proc Natl Acad Sci U S A* **110**, 743–748 (2013).
885 50. Chojnacki, J. *et al.* Envelope glycoprotein mobility on HIV-1 particles depends on
886 the virus maturation state. *Nat Commun* **8**, (2017).
887 51. Hart, T. K., Klinkner, A. M., Ventre, J. & Bugelski, P. J. Morphometric analysis
888 of envelope glycoprotein gp120 distribution on HIV-1 virions. *J Histochem*
889 *Cytochem* **41**, 265–271 (1993).
890 52. Zhu, P. *et al.* Electron tomography analysis of envelope glycoprotein trimers on
891 HIV and simian immunodeficiency virus virions. *Proc Natl Acad Sci U S A* **100**,
892 15812–15817 (2003).
893 53. Zhu, P. *et al.* Distribution and three-dimensional structure of AIDS virus envelope
894 spikes. *Nature* **441**, 847–852 (2006).
895 54. Murakami, T., Ablan, S., Freed, E. O. & Tanaka, Y. Regulation of human
896 immunodeficiency virus type 1 Env-mediated membrane fusion by viral protease
897 activity. *J Virol* **78**, 1026–1031 (2004).
898 55. Wyma, D. J. *et al.* Coupling of human immunodeficiency virus type 1 fusion to
899 virion maturation: a novel role of the gp41 cytoplasmic tail. *J Virol* **78**, 3429–3435
900 (2004).
901 56. Rauh, N. R., Schmidt, A., Bormann, J., Nigg, E. A. & Mayer, T. U. Calcium
902 triggers exit from meiosis II by targeting the APC/C inhibitor XErp1 for
903 degradation. *Nature* **437**, 1048–1052 (2005).
904 57. Singer, I. I. *et al.* CCR5, CXCR4, and CD4 are clustered and closely apposed on
905 microvilli of human macrophages and T cells. *J Virol* **75**, 3779–3790 (2001).
906 58. Abramson, J. *et al.* Accurate structure prediction of biomolecular interactions with
907 AlphaFold 3. *Nature* **630**, 493–500 (2024).
908 59. Basmaciogullari, S., Pacheco, B., Bour, S. & Sodroski, J. Specific interaction of
909 CXCR4 with CD4 and CD8alpha: functional analysis of the CD4/CXCR4

interaction in the context of HIV-1 envelope glycoprotein-mediated membrane fusion. *Virology* **353**, 52–67 (2006).

60. Zaitseva, M. *et al.* Increased CXCR4-dependent HIV-1 fusion in activated T cells: role of CD4/CXCR4 association. *J Leukoc Biol* **78**, 1306–1317 (2005).
61. Lapham, C. K., Zaitseva, M. B., Lee, S., Romanstseva, T. & Golding, H. Fusion of monocytes and macrophages with HIV-1 correlates with biochemical properties of CXCR4 and CCR5. *Nat Med* **5**, 303–308 (1999).
62. Lee, S. *et al.* Coreceptor competition for association with CD4 may change the susceptibility of human cells to infection with T-tropic and macrophagetropic isolates of human immunodeficiency virus type 1. *J Virol* **74**, 5016–5023 (2000).
63. Hoxie, J. A. *et al.* Alterations in T4 (CD4) protein and mRNA synthesis in cells infected with HIV. *Science* **234**, 1123–1127 (1986).
64. Potash, M. J. & Volsky, D. J. Viral Interference in HIV-1 Infected Cells. *Rev. Med. Virol* **8**, 203–211 (1998).
65. Chenine, A. L., Sattentau, Q. & Moulard, M. Selective HIV-1-induced downmodulation of CD4 and coreceptors. *Arch Virol* **145**, 455–471 (2000).
66. Choi, B. *et al.* Down-regulation of cell surface CXCR4 by HIV-1. *Virol J* **5**, (2008).
67. Balabanian, K. *et al.* WHIM syndromes with different genetic anomalies are accounted for by impaired CXCR4 desensitization to CXCL12. *Blood* **105**, 2449–2457 (2005).
68. Wyatt, R. & Sodroski, J. The HIV-1 envelope glycoproteins: fusogens, antigens, and immunogens. *Science* **280**, 1884–1888 (1998).
69. Blumenthal, R., Durell, S. & Viard, M. HIV entry and envelope glycoprotein-mediated fusion. *J Biol Chem* **287**, 40841–40849 (2012).
70. Chen, B. Molecular Mechanism of HIV-1 Entry. *Trends Microbiol* **27**, 878–891 (2019).
71. Traunecker, A., Schneider, J., Kiefer, H. & Karjalainen, K. Highly efficient neutralization of HIV with recombinant CD4-immunoglobulin molecules. *Nature* **339**, 68–70 (1989).
72. Nara, P. L., Hwang, K. M., Rausch, D. M., Lifson, J. D. & Eiden, L. E. CD4 antigen-based antireceptor peptides inhibit infectivity of human immunodeficiency virus in vitro at multiple stages of the viral life cycle. *Proc Natl Acad Sci U S A* **86**, 7139–7143 (1989).
73. Schooley, R. T. *et al.* Recombinant soluble CD4 therapy in patients with the acquired immunodeficiency syndrome (AIDS) and AIDS-related complex. A phase I-II escalating dosage trial. *Ann Intern Med* **112**, 247–253 (1990).
74. Kahn, J. O. *et al.* The safety and pharmacokinetics of recombinant soluble CD4 (rCD4) in subjects with the acquired immunodeficiency syndrome (AIDS) and AIDS-related complex. A phase 1 study. *Ann Intern Med* **112**, 254–261 (1990).
75. Hoffmann, M. A. G. *et al.* Nanoparticles presenting clusters of CD4 expose a universal vulnerability of HIV-1 by mimicking target cells. *Proc Natl Acad Sci U S A* **117**, 18719–18728 (2020).
76. Schamel, W. W. A. & Alarcón, B. Organization of the resting TCR in nanoscale oligomers. *Immunol Rev* **251**, 13–20 (2013).
77. Razvag, Y. *et al.* T Cell Activation through Isolated Tight Contacts. *Cell Rep* **29**, 3506-3521.e6 (2019).
78. Lillemeier, B. F. *et al.* TCR and Lat are expressed on separate protein islands on T cell membranes and concatenate during activation. *Nat Immunol* **11**, 90–96 (2010).
79. Verstreken, P. & Bellen, H. J. Meaningless minis? Mechanisms of neurotransmitter-receptor clustering. *Trends Neurosci* **25**, 383–385 (2002).

960 80. Germain, R. N. T-cell signaling: the importance of receptor clustering. *Curr Biol*
961 **7**, (1997).
962 81. Cairo, C. W. Signaling by committee: receptor clusters determine pathways of
963 cellular activation. *ACS Chem Biol* **2**, 652–655 (2007).
964 82. Chang, M. I., Panorchan, P., Dobrowsky, T. M., Tseng, Y. & Wirtz, D. Single-
965 molecule analysis of human immunodeficiency virus type 1 gp120-receptor
966 interactions in living cells. *J Virol* **79**, 14748–14755 (2005).
967 83. Cézanne, L. *et al.* Dynamic confinement of NK2 receptors in the plasma
968 membrane. Improved FRAP analysis and biological relevance. *J Biol Chem* **279**,
969 45057–45067 (2004).
970 84. Jacquier, V., Prummer, M., Segura, J. M., Pick, H. & Vogel, H. Visualizing odorant
971 receptor trafficking in living cells down to the single-molecule level. *Proc Natl*
972 *Acad Sci U S A* **103**, 14325–14330 (2006).
973 85. Bray, D. Protein molecules as computational elements in living cells. *Nature* **376**,
974 307–312 (1995).
975 86. Cho, W. & Stahelin, R. V. Membrane-protein interactions in cell signaling and
976 membrane trafficking. *Annu Rev Biophys Biomol Struct* **34**, 119–151 (2005).
977 87. Gurry, T., Kahramanoğullari, O. & Endres, R. G. Biophysical mechanism for ras-
978 nanocluster formation and signaling in plasma membrane. *PLoS One* **4**, (2009).
979 88. Popik, W., Hesselgesser, J. E. & Pitha, P. M. Binding of human immunodeficiency
980 virus type 1 to CD4 and CXCR4 receptors differentially regulates expression of
981 inflammatory genes and activates the MEK/ERK signaling pathway. *J Virol* **72**,
982 6406–6413 (1998).
983 89. Davis, C. B. *et al.* Signal transduction due to HIV-1 envelope interactions with
984 chemokine receptors CXCR4 or CCR5. *J Exp Med* **186**, 1793–1798 (1997).
985 90. Pasquereau, S. & Herbein, G. CounterAKTing HIV: Toward a 'Block and Clear'
986 Strategy? *Front Cell Infect Microbiol* **12**, (2022).
987 91. François, F. & Klotman, M. E. Phosphatidylinositol 3-kinase regulates human
988 immunodeficiency virus type 1 replication following viral entry in primary CD4+
989 T lymphocytes and macrophages. *J Virol* **77**, 2539–2549 (2003).
990 92. Deng, J. *et al.* HIV Envelope gp120 Alters T Cell Receptor Mobilization in the
991 Immunological Synapse of Uninfected CD4 T Cells and Augments T Cell
992 Activation. *J Virol* **90**, 10513–10526 (2016).
993 93. Chertova, E. *et al.* Envelope glycoprotein incorporation, not shedding of surface
994 envelope glycoprotein (gp120/SU), Is the primary determinant of SU content of
995 purified human immunodeficiency virus type 1 and simian immunodeficiency
996 virus. *J Virol* **76**, 5315–5325 (2002).
997 94. DeSantis, M. C., Kim, J. H., Song, H., Klasse, P. J. & Cheng, W. Quantitative
998 Correlation between Infectivity and Gp120 Density on HIV-1 Virions Revealed by
999 Optical Trapping Virometry. *J Biol Chem* **291**, 13088–13097 (2016).
1000 95. García-Cuesta, E. M. *et al.* Allosteric modulation of the CXCR4:CXCL12 axis by
1001 targeting receptor nanoclustering via the TMV-TMVI domain. *Elife* **13**, (2024).
1002 96. Hernandez, P. A. *et al.* Mutations in the chemokine receptor gene CXCR4 are
1003 associated with WHIM syndrome, a combined immunodeficiency disease. *Nat*
1004 *Genet* **34**, 70–74 (2003).
1005 97. Kumar, R. *et al.* Reduced G protein signaling despite impaired internalization and
1006 β-arrestin recruitment in patients carrying a CXCR4Leu317fsX3 mutation causing
1007 WHIM syndrome. *JCI Insight* **8**, (2023).
1008 98. Geleziunas, R., Bour, S. & Wainberg, M. A. Cell surface down-modulation of CD4
1009 after infection by HIV-1. *FASEB J* **8**, 593–600 (1994).

1010 99. Hubert, P., Bismuth, G., Körner, M. & Debré, P. HIV-1 glycoprotein gp120
1011 disrupts CD4-p56lck/CD3-T cell receptor interactions and inhibits CD3 signaling.
1012 *Eur J Immunol* **25**, 1417–1425 (1995).
1013 100. Daecke, J., Fackler, O. T., Dittmar, M. T. & Kräusslich, H.-G. Involvement of
1014 clathrin-mediated endocytosis in human immunodeficiency virus type 1 entry. *J*
1015 *Virol* **79**, 1581–1594 (2005).
1016 101. Aggarwal, A. *et al.* HIV infection is influenced by dynamin at 3 independent points
1017 in the viral life cycle. *Traffic* **18**, 392–410 (2017).
1018 102. de la Vega, M. *et al.* Inhibition of HIV-1 endocytosis allows lipid mixing at the
1019 plasma membrane, but not complete fusion. *Retrovirology* **8**, 99 (2011).
1020 103. Miyauchi, K., Kim, Y., Latinovic, O., Morozov, V. & Melikyan, G. B. HIV enters
1021 cells via endocytosis and dynamin-dependent fusion with endosomes. *Cell* **137**,
1022 433–444 (2009).
1023 104. Carter, G. C., Bernstone, L., Baskaran, D. & James, W. HIV-1 infects macrophages
1024 by exploiting an endocytic route dependent on dynamin, Rac1 and Pak1. *Virology*
1025 **409**, 234–250 (2011).
1026 105. Van Wilgenburg, B., Moore, M. D., James, W. S. & Cowley, S. A. The productive
1027 entry pathway of HIV-1 in macrophages is dependent on endocytosis through lipid
1028 rafts containing CD4. *PLoS One* **9**, (2014).
1029 106. Popik, W., Alce, T. M. & Au, W.-C. Human immunodeficiency virus type 1 uses
1030 lipid raft-colocalized CD4 and chemokine receptors for productive entry into
1031 CD4(+) T cells. *J Virol* **76**, 4709–4722 (2002).
1032 107. Neel, N. F., Schutyser, E., Sai, J., Fan, G. H. & Richmond, A. Chemokine receptor
1033 internalization and intracellular trafficking. *Cytokine Growth Factor Rev* **16**, 637–
1034 658 (2005).
1035 108. Gardeta, S. R. *et al.* Sphingomyelin Depletion Inhibits CXCR4 Dynamics and
1036 CXCL12-Mediated Directed Cell Migration in Human T Cells. *Front Immunol* **13**,
1037 (2022).
1038 109. Hauser, M. A. *et al.* Inflammation-Induced CCR7 Oligomers Form Scaffolds to
1039 Integrate Distinct Signaling Pathways for Efficient Cell Migration. *Immunity* **44**,
1040 59–72 (2016).
1041 110. Harrop, H. A. & Rider, C. C. Heparin and its derivatives bind to HIV-1
1042 recombinant envelope glycoproteins, rather than to recombinant HIV-1 receptor,
1043 CD4. *Glycobiology* **8**, 131–137 (1998).
1044 111. Mondor, I., Ugolini, S. & Sattentau, Q. J. Human immunodeficiency virus type 1
1045 attachment to HeLa CD4 cells is CD4 independent and gp120 dependent and
1046 requires cell surface heparans. *J Virol* **72**, 3623–3634 (1998).
1047 112. Saphire, A. C. S., Bobardt, M. D., Zhang, Z., David, G. & Gallay, P. A. Syndecans
1048 serve as attachment receptors for human immunodeficiency virus type 1 on
1049 macrophages. *J Virol* **75**, 9187–9200 (2001).
1050 113. Moulard, M. *et al.* Selective interactions of polyanions with basic surfaces on
1051 human immunodeficiency virus type 1 gp120. *J Virol* **74**, 1948–1960 (2000).
1052 114. Ugolini, S., Mondor, I. & Sattentau, Q. J. HIV-1 attachment: another look. *Trends*
1053 *Microbiol* **7**, 144–149 (1999).
1054 115. Dobrowsky, T. M., Zhou, Y., Sun, S. X., Siliciano, R. F. & Wirtz, D. Monitoring
1055 early fusion dynamics of human immunodeficiency virus type 1 at single-molecule
1056 resolution. *J Virol* **82**, 7022–7033 (2008).
1057 116. Rabenstein, D. L. Heparin and heparan sulfate: structure and function. *Nat Prod*
1058 *Rep* **19**, 312–331 (2002).
1059

1060
1061 **Figure Legends**

1062

1063 **Figure 1. X4-gp120 modulates CXCR4 dynamics and nanoclustering.** Single-particle
1064 tracking analysis of JKCD4^{+}X4^{-} cells transiently transfected with CXCR4-AcGFP on
1065 fibronectin (FN)-, FN + CXCL12-, or FN + X4-gp120-coated coverslips (828 particles in
1066 96 cells on FN; 2,997 in 95 cells on FN + CXCL12 and 1,547 in 91 cells on FN + X4-
1067 gp120) n = 3. **A)** Percentage of mobile and immobile CXCR4-AcGFP particles at the
1068 membrane of cells treated as indicated. **B)** Diffusion coefficients ($D_{1–4}$) of mobile
1069 particles at the membrane of cells treated as indicated with the median value of each
1070 experiment (black circles) and the median of all trajectories (dotted black lines). (****p
1071 ≤ 0.0001). **C)** Frequency of CXCR4-AcGFP particles containing monomers and dimers
1072 (≤2) or nanoclusters (≥3), mean ± SD calculated from mean spot intensity (MSI) values
1073 of each particle as compared with the value of monomeric CD86-AcGFP (980 ± 86 a.u.,
1074 **p ≤ 0.01, ***p ≤ 0.001). **D)** Intensity distribution of individual CXCR4-AcGFP
1075 trajectories on unstimulated and CXCL12 or X4-gp120-stimulated cells. Graph shows the
1076 distribution of all trajectories, with the mean value of each experiment (black circles) and
1077 the median of all trajectories (dotted black lines) (n = 3; ****p ≤ 0.0001).

1078

1079 **Figure 2. gp120-VLPs are mature particles that express a low number of Env**
1080 **trimers. A)** Representative images of clarified VLPs visualized by STED microscopy.
1081 Upper panels show images of the indicated VLPs stained for Gag p24 (blue) and gp120
1082 (red). Lower panels show 10× magnification of equivalent images. White arrows indicate
1083 mature VLPs (p24 condensation). (**B)** Percentage of mature VLPs, analyzed from the
1084 images in A) using TrackAnalyzer in ImageJ, based on p24 intensity and aggregation
1085 level (mean ± SD; n = 2; ****p ≤ 0.0001; the significance indicated on immature VLPs
1086 bar shows the difference with all other conditions). **C)** Percentage of VLPs expressing
1087 gp120 on their surface, as analyzed in ImageJ (mean ± SD; n = 2; ***p ≤ 0.001). **D)**
1088 Distribution of gp120 mean fluorescence intensity. Each spot corresponds to the mean
1089 fluorescence intensity for each analyzed VLP in a.u. The black line represents the mean
1090 of all values (**** p ≤ 0.0001). **E)** Frequency of gp120 intensity/particle. Statistical
1091 significance was determined by one-way-ANOVA followed by Tukey's multiple
1092 comparisons test in panels B and C and by Mann-Whitney analysis for panel D.

1093

1094 **Figure 3. gp120 VLPs modulates CXCR4 dynamics and nanoclustering.** Single-
1095 particle tracking analysis of JKCD4^{+}X4^{-} cells transiently transfected with CXCR4-
1096 AcGFP, on fibronectin (FN)-, FN + VLPs-, or FN + gp120 VLPs-coated coverslips (1,087
1097 particles in 159 cells on FN; 1,400 in 153 cells on FN +VLPs and 1,061 in 160 cells on
1098 FN + gp120 VLPs) n = 6. **A)** Diffusion coefficients (D_{1-4}) of mobile particles at the
1099 membrane of cells treated as indicated. Figure shows the mean value of each experiment
1100 (black circles) and the median of all trajectories (dotted black lines) (n = 6; ****p ≤
1101 0.0001). **B)** Frequency of CXCR4-AcGFP particles containing monomers and dimers
1102 (≤2) or nanoclusters (≥3) in cells treated as indicated. Mean ± SD calculated from mean
1103 spot intensity (MSI) values of each particle as compared with the value of monomeric
1104 CD86-AcGFP (980 ± 86 a.u., **p ≤ 0.05, **p ≤ 0.01, ****p ≤ 0.0001). **C)** Intensity
1105 distribution (arbitrary units, a.u.) from individual CXCR4-AcGFP trajectories on cells
1106 treated as indicated. Graph shows the distribution of all trajectories, with the mean value
1107 of each experiment (black circles) and the median of all trajectories (dotted black lines)
1108 (n = 6; ****p ≤ 0.0001).
1109
1110 **Figure 4. gp120 VLPs modulate CXCR4^{R334X} dynamics and nanoclustering.** Single-
1111 particle tracking analysis of JKCD4^{+}X4^{-} cells transiently transfected with CXCR4^{R334X}-
1112 AcGFP, on fibronectin (FN)-, FN + VLPs-, or FN + gp120 VLPs-coated coverslips (341
1113 particles in 63 cells on FN; 610 in 54 cells on FN + VLPs and 707 in 63 cells on FN +
1114 gp120 VLPs) n = 2. **A)** Intensity distribution (arbitrary units, a.u.) from individual
1115 CXCR4^{R334X}-AcGFP trajectories on cells treated as indicated. Graph shows the
1116 distribution of all trajectories, with the mean value of each experiment (black circles) and
1117 the median of all trajectories ± SD (dotted black lines) (n = 2; ****p ≤ 0.0001). **B)**
1118 Diffusion coefficients (D_{1-4}) of mobile single particle trajectories at the membrane of cells
1119 treated as indicated. Figure shows the mean value of each experiment (black circles) and
1120 the median of all trajectories (dotted black lines) (n = 2; n.s. not significant, *p ≤ 0.05,
1121 ****p ≤ 0.0001). **C)** Frequency of CXCR4^{R334X}-AcGFP particles containing monomers
1122 plus dimers (≤2) or nanoclusters (≥3), ± SD calculated from mean spot intensity values
1123 of each particle as compared with the value of monomeric CD86-AcGFP (*p ≤ 0.05, ***p
1124 ≤ 0.001).
1125
1126 **Figure 5. CD4 forms heterodimers with CXCR4 and CXCR4^{R334X}.** FRET saturation
1127 curves generated using HEK-293T cells transiently transfected with a constant amount of

1128 CD4-CFP DNA (2 μg) and increasing amounts of **A)** CXCR4-YFP (0.5–8.0 μg), **B)**
1129 $CXCR4^{R334X}$-YFP (0.5–8.0 μg) or **C)** $5HT_{2B}$ DNA (0.5–12 μg). K_D and $FRET_{max}$ values
1130 were calculated using a nonlinear regression equation for a single binding-site model (n
1131 = 2). **D)** FRET efficiency in HEK-293 cells transiently transfected with CXCR4-YFP/
1132 CD4-CFP (ratio 15:9), in the absence or presence of gp120 VLPs or empty VLPs. Data
1133 shows FRET efficiency (arbitrary units, a.u.) (mean ± SD; n = 3; n.s. not significant, *p
1134 ≤ 0.05, ***p ≤ 0.001). **E)** FRET efficiency in HEK-293 cells transiently transfected with
1135 $CXCR4^{R334X}$-YFP/CD4-CFP (ratio 15:9), in the absence or presence of gp120-VLPs or
1136 empty VLPs. Data shows FRET efficiency (a.u.) (mean ± SD; n = 3; n.s. not significant,
1137 *p ≤ 0.05, ***p ≤ 0.001, **** p ≤ 0.0001).
1138
1139
1140 **Figure 6. X4-gp120 promote similar internalization patterns of CXCR4 and**
1141 **$CXCR4^{R334X}$ receptors. A)** Surface receptor expression of CXCR4 (white dots) or
1142 $CXCR4^{R334X}$ (black dots), after stimulation with CXCL12 (blue lines) or X4-gp120 (red
1143 lines). Results show mean ± SD of the percentage of receptor expression at the cell surface
1144 (n = 3). **B)** Surface receptor expression of CD4 in JK $CD4^+$ $CXCR4^+$ (white dots) or JK
1145 $CD4^+$ $CXCR4^{R334X}$ (black dots), after stimulation with CXCL12 (blue lines) or X4-gp120
1146 (red lines). Results show mean ± SD of the percentage of receptor expression at the cell
1147 surface (n = 3). Statistical significance was determined by two-way-ANOVA (n.s. not
1148 significant ,*p ≤ 0.05, **p ≤ 0.01, ***p ≤ 0.001, **** p ≤ 0.0001).
1149
1150 **Figure 7. CD4/CXCR4 and CD4/$CXCR4^{R334X}$ complexes support similar HIV-1**
1151 **infection.** The presence of $CXCR4^{R334X}$ on $JKCD4^+$ cells does not alter gp120 binding
1152 and increases fusion events with target cells expressing HIV pHXB2 envelope. **A)**
1153 Binding of X4-gp120 to target cells expressing CD4 and CXCR4 or CD4 and
1154 $CXCR4^{R334X}$ analyzed by flow cytometry. Cells were incubated with 0.3 μg/mL of X4-
1155 gp120 at 37ºC for 30 minutes. Data show MFI (arbitrary units, a.u.) mean ± SD; (n = 2).
1156 Statistical significance was determined using Student's t-test (n.s.= not significant). **B)**
1157 Cell-cell fusion between JKHXBc2-expressing HIV-1 envelope and different target cells
1158 ($JKCD4^+CXCR4^+$, $JKCD4^+CXCR4^-$ and $JKCD4^+CXCR4^{R334X}$). Prior to co-culture, each
1159 cell type was loaded with the corresponding cell-tracker. Data show the percentage of
1160 fusion events ± SD (n = 6). We used as reference the fusions events detected in
1161 $JKCD4^+CXCR4^+$ cells (100%). Statistical significance was determined by one-way-

1162 ANOVA (*$p < 0.05$, ****$p \leq 0.0001$). **C**) Representative biparametric histograms from
1163 cells in B showing CMAC *versus* orange fluorophores. **D**) Human PBMCs isolated from
1164 a WHIM patient (WHIM) and three healthy donors (HD1-3) in two independent
1165 experiments were infected with X4-pseudotyped HIV-1_{NL4-3} (MOI: 0.001). At 2 hours
1166 post infection (p.i.), supernatant samples were obtained at different time points (days
1167 post-infection) and p24 levels (pg/mL) in each sample were determined using a
1168 commercial ELISA. Results show mean ± SD (n = 2).
1169

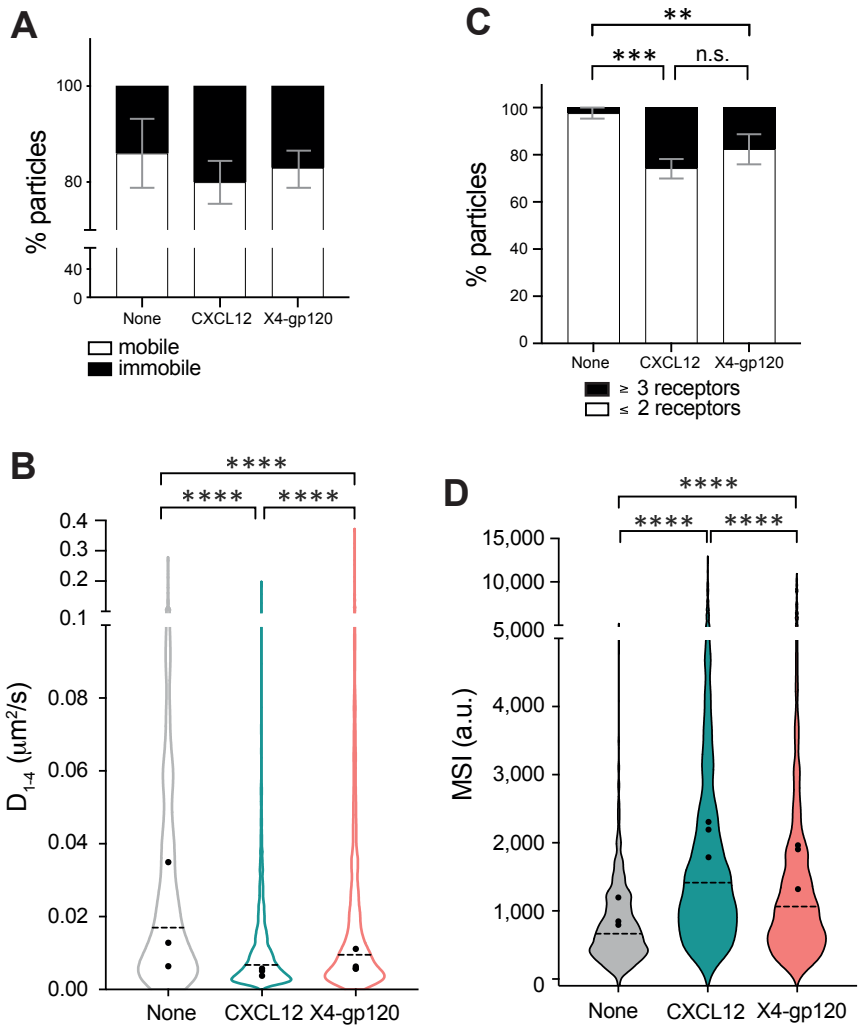
A
% particles
100
80
40
0
None
CXCL12
X4-gp120
mobile
immobile
C
**
***
n.s.
% particles
100
80
60
40
20
0
None
CXCL12
X4-gp120
≥ 3 receptors
≤ 2 receptors
B
****
****
****
D1-4 (µm²/s)
0.4
0.3
0.2
0.1
0.08
0.06
0.04
0.02
0.00
None
CXCL12
X4-gp120
D
****
****
****
MSI (a.u.)
15,000
10,000
5,000
4,000
3,000
2,000
1,000
0
None
CXCL12
X4-gp120

Figure 1

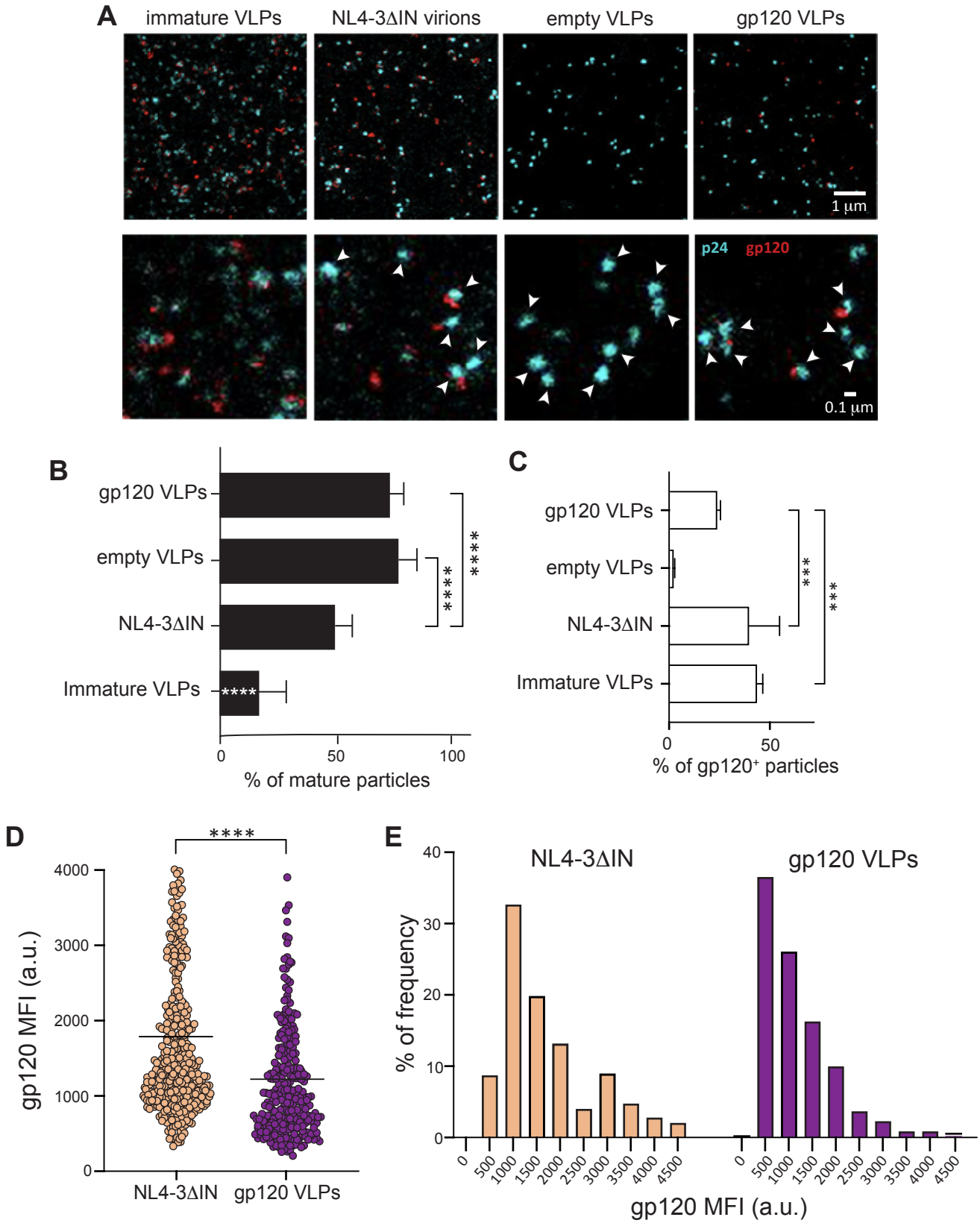
A
immature VLPs
NL4-3ΔIN virions
empty VLPs
gp120 VLPs
1 µm
p24
gp120
0.1 µm
B
gp120 VLPs
empty VLPs
NL4-3ΔIN
Immature VLPs
****
0
50
100
% of mature particles
C
gp120 VLPs
empty VLPs
NL4-3ΔIN
Immature VLPs
***
0
50
% of gp120⁺ particles
D
****
gp120 MFI (a.u.)
4000
3000
2000
1000
0
NL4-3ΔIN
gp120 VLPs
E
NL4-3ΔIN
gp120 VLPs
% of frequency
40
30
20
10
0
0
500
1000
1500
2000
2500
3000
3500
4000
4500
gp120 MFI (a.u.)

Figure 2

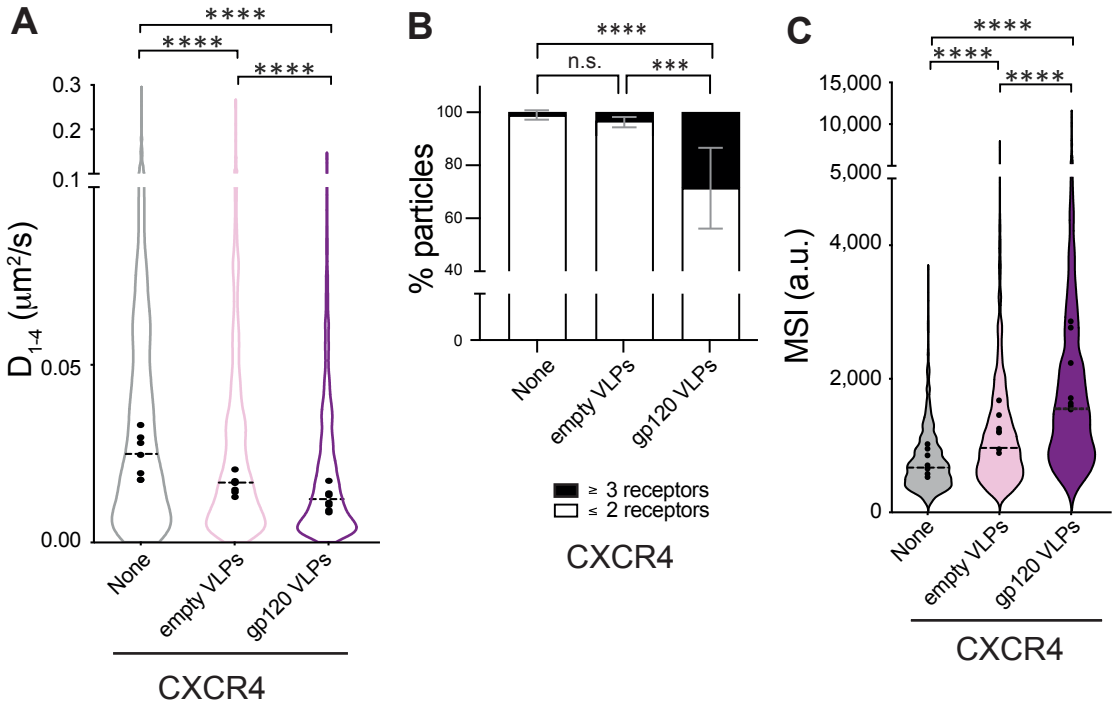
A
****
****
****
0.3
0.2
0.1
0.05
0.00
D1-4 (µm2/s)
None
empty VLPs
gp120 VLPs
CXCR4
B
****
n.s.
***
100
80
60
40
0
% particles
None
empty VLPs
gp120 VLPs
≥ 3 receptors
≤ 2 receptors
CXCR4
C
****
****
****
15,000
10,000
5,000
4,000
2,000
0
MSI (a.u.)
None
empty VLPs
gp120 VLPs
CXCR4

Figure 3

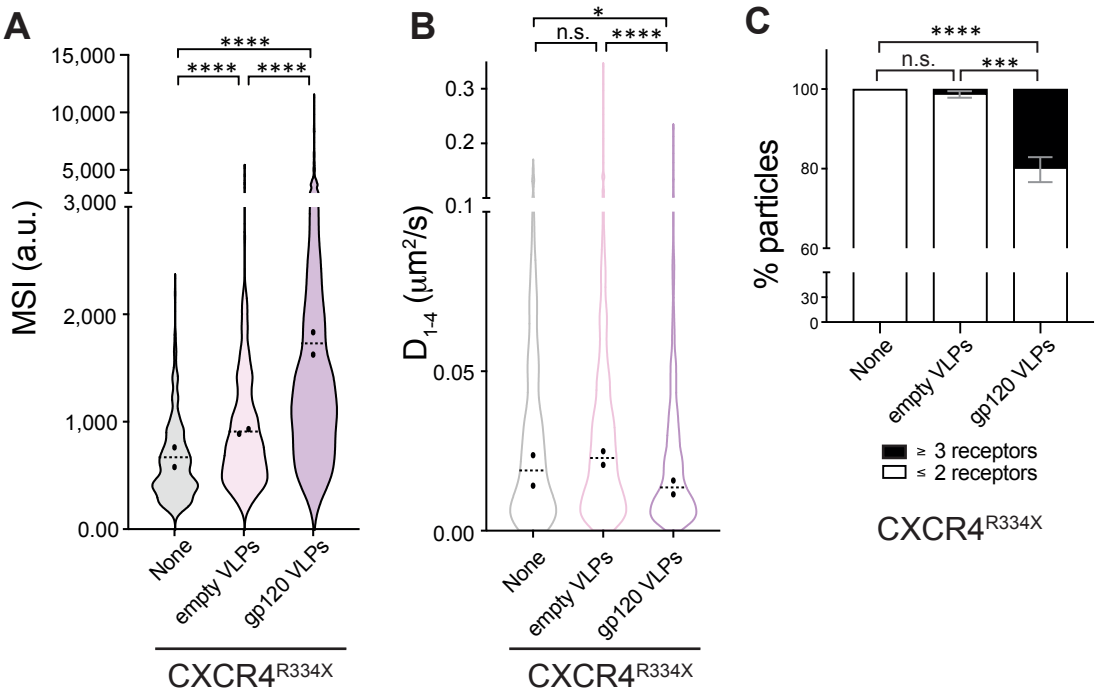
A
MSI (a.u.)
15,000
10,000
5,000
3,000
2,000
1,000
0.00
****
****
****
None
empty VLPs
gp120 VLPs
CXCR4R334X
B
D1-4 (µm2/s)
0.3
0.2
0.1
0.05
0.00
*
n.s.
****
None
empty VLPs
gp120 VLPs
CXCR4R334X
C
% particles
100
80
60
30
0
****
n.s.
***
None
empty VLPs
gp120 VLPs
≥ 3 receptors
≤ 2 receptors
CXCR4R334X

Figure 4

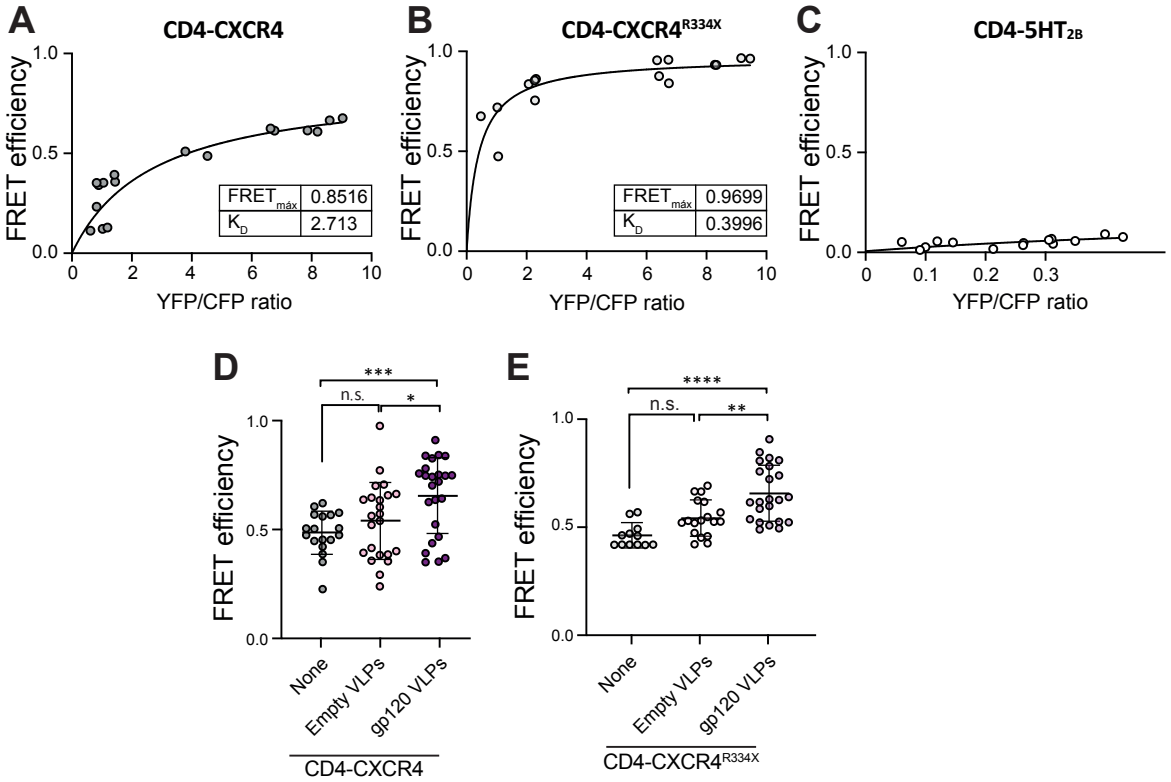
A
CD4-CXCR4
FRET efficiency
YFP/CFP ratio
FRETmáx 0.8516
KD 2.713
B
CD4-CXCR4R334X
FRET efficiency
YFP/CFP ratio
FRETmáx 0.9699
KD 0.3996
C
CD4-5HT2B
FRET efficiency
YFP/CFP ratio
D
FRET efficiency
***
n.s.
*
None
Empty VLPs
gp120 VLPs
CD4-CXCR4
E
FRET efficiency
****
n.s.
**
None
Empty VLPs
gp120 VLPs
CD4-CXCR4R334X

Figure 5

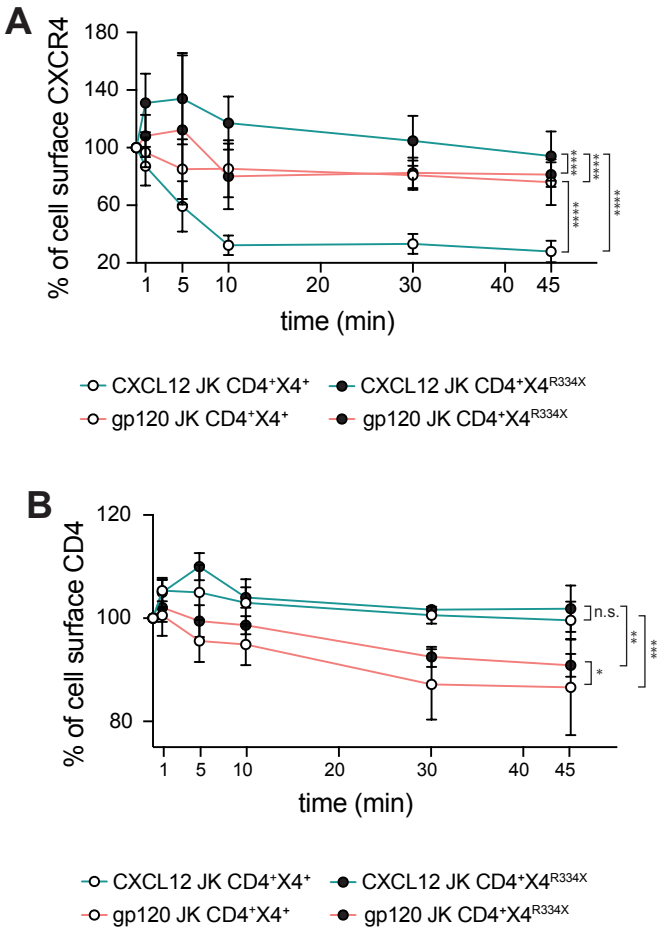
A
% of cell surface CXCR4
180
140
100
60
20
1
5
10
20
30
40
45
time (min)
****
****
****
****
CXCL12 JK CD4+X4+
CXCL12 JK CD4+X4R334X
gp120 JK CD4+X4+
gp120 JK CD4+X4R334X
B
% of cell surface CD4
120
100
80
1
5
10
20
30
40
45
time (min)
n.s.
**
***
*
CXCL12 JK CD4+X4+
CXCL12 JK CD4+X4R334X
gp120 JK CD4+X4+
gp120 JK CD4+X4R334X

Figure 6

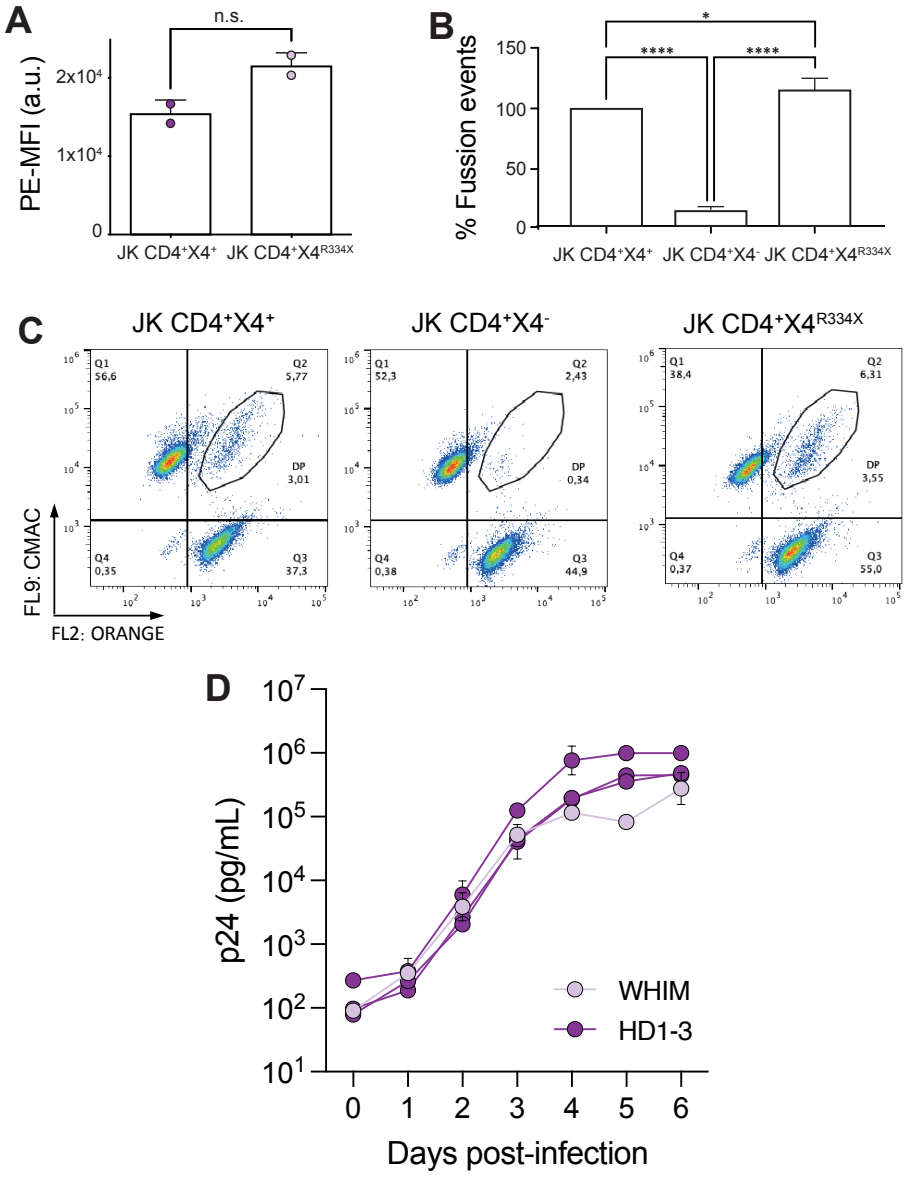
A
n.s.
PE-MFI (a.u.)
2x10⁴
1x10⁴
0
JK CD4⁺X4⁺
JK CD4⁺X4R334X
B
*
****
****
% Fussion events
150
100
50
0
JK CD4⁺X4⁺
JK CD4⁺X4⁻
JK CD4⁺X4R334X
C
JK CD4⁺X4⁺
JK CD4⁺X4⁻
JK CD4⁺X4R334X
Q1 56,6
Q2 5,77
DP 3,01
Q4 0,35
Q3 37,3
Q1 52,3
Q2 2,43
DP 0,34
Q4 0,38
Q3 44,9
Q1 38,4
Q2 6,31
DP 3,55
Q4 0,37
Q3 55,0
FL9: CMAC
FL2: ORANGE
D
p24 (pg/mL)
10⁷
10⁶
10⁵
10⁴
10³
10²
10¹
0
1
2
3
4
5
6
Days post-infection
WHIM
HD1-3

Figure 7